

Journal of Mechanics of Materials and Structures

**COLLAPSE MECHANISMS OF METALLIC SANDWICH STRUCTURES WITH
ALUMINUM FOAM-FILLED CORRUGATED CORES**

Bin Han, Lei L. Yan, Bo Yu, Qian C. Zhang, Chang Q. Chen and Tian J. Lu

Volume 9, No. 4

July 2014



COLLAPSE MECHANISMS OF METALLIC SANDWICH STRUCTURES WITH ALUMINUM FOAM-FILLED CORRUGATED CORES

BIN HAN, LEI L. YAN, BO YU, QIAN C. ZHANG, CHANG Q. CHEN AND TIAN J. LU

The physical mechanisms underlying the beneficial effect of filling aluminum foams into the interstices of corrugated plates made of stainless steel were explored with finite element (FE) simulations. Relative to unfilled corrugated plates of equal mass, this effect was assessed on the basis of elevated peak stress and enhanced energy absorption under quasistatic out-of-plane compression. Upon validating the FE predictions against existing measurements, the influence of key geometrical and material parameters on the compressive response of foam-filled corrugated plates was investigated. Different from the traditional buckling modes of empty corrugations, four new buckling modes were identified for foam-filled corrugations. Based upon these deformation modes of post-buckling, collapse mechanism maps were constructed. Due to the additional resistance provided by foam filling against buckling of the corrugated plate and the strengthening of foam insertions due to complex stressing, both the load bearing capacity and energy absorption of foam-filled sandwiches were greatly enhanced.

1. Introduction

Although not the best structural material, metallic and polymer foams with stochastic cellular topologies have been widely exploited for energy absorption, heat dissipation, vibration damping and other functional applications. In recent years, there is also a growing interest in exploiting the stochastic foams as a filling material to enhance simultaneously the load-bearing and energy absorption capabilities of traditional lightweight structures, such as hollow tubes and sandwich constructions having flow-through, periodic lattice truss cores [Vaziri et al. 2006; Mamalis et al. 2008; Kazemahvazi and Zenkert 2009; Kazemahvazi et al. 2009; Nia and Sadeghi 2010; Ostos et al. 2012; Zhang et al. 2013; Yan et al. 2013]. From the viewpoint of energy absorption, in the field of civil engineering (structural mechanics in particular), structures that deform plastically under static or dynamic compression have been characterized into two main types [Calladine and English 1984; Tam and Calladine 1991]. A type I structure (radially loaded arches and rings, say) exhibits a plateau-like stress versus strain curve and is able to absorb large amount of energy at a constant stress level, thus a preferable candidate for energy absorption. In contrast, the stress of a type II structure (axially loaded columns, for example) drops sharply after the peak value is reached, thus less attractive for energy absorption applications because large forces are transferred while limited amount of energy is absorbed. Under quasistatic out-of-plane compression, it has been established that inserting close-celled aluminum foams into the interstices of a metallic corrugate-cored sandwich panel increases significantly both its peak stress and energy absorption [Yan et al. 2013]. Further, with foam insertion, the initially type II energy absorbing structure (i.e., empty corrugated cores)

Keywords: foam-filled corrugated core, finite element method, buckling, collapse mechanism.

was transformed into a type I energy absorbing structure, enabling high crushing strength and high energy absorption per unit mass.

1.1. Previous research on foam-filled sandwich constructions. Before discussing the effect of aluminum foam filling upon the mechanical properties of corrugated plates, consider first the case of combining foam with various types of pin-reinforcement for sandwich constructions. The effect of titanium and carbon fiber pin-reinforcements upon the out-of-plane compressive strength of polymethacrylimide foam-cored sandwich panels was measured both quasistatically and dynamically [Cartié and Fleck 2003]. It was found that the compressive strength was governed by elastic buckling of the pins, with the foam core behaving as an elastic Winkler foundation in supporting the pins. As a result, the pin-reinforced core had a strength and energy absorption capacity in excess of the combined individual contributions from the foam and unsupported pins. Subsequently, Marasco et al. [2006] measured the out-of-plane properties of two different Z-pinned sandwich panels, both filled with Rohacell foam, under quasistatic tension, shear, or compression. Compared with equivalent honeycomb cores, the foam supported Z-pin cores exhibited higher specific stiffness but lower strength. Similar experimental measurements for Z-pinned composite sandwich panels were carried out by Nanayakkara et al. [2011]. The collapse of X-core sandwich panels consisting of a pin reinforced polymer foam core and carbon fiber face sheets were assessed experimentally under three-point bending [Rice et al. 2006]. Compared with other sandwich cores such as aluminum honeycombs and aluminum foams, it was found that such an X-core led to higher bending stiffness and strength. Liu et al. [2008] developed a comprehensive analytical model to characterize the collapse behavior of pin-reinforced foam sandwich beams under 3-point bending and verified the model predictions against finite element (FE) simulation results. It was demonstrated that sandwich beams with pin-reinforced polymer foam cores were structurally more efficient than foam-cored sandwich beams without pin reinforcements.

Consider next the influence of foam filling upon the mechanical performance of sandwich panels having other core types such as corrugated plates, honeycombs, egg boxes, and 3D lattice trusses. The performance of a hierarchical all-composite corrugated sandwich core filled with PMI-foam (Rohacell) was investigated analytically and experimentally [Kazemahvazi and Zenkert 2009; Kazemahvazi et al. 2009]. Dependent upon the geometrical dimensions and material properties of the sandwich, a multitude of failure modes were identified. It was found that the weight specific strength of a well-designed hierarchical structure could be 7 times higher than that of its monolithic counterpart. The enhancement in strength was attributed mainly to the increased buckling resistance of the hierarchical core members due to foam support, especially for core configurations with low overall density. As the core density was increased, the monolithic core members became stockier and more resistant to buckling and thus the benefits of the hierarchical structure were gradually lost.

Nia and Sadeghi [2010] investigated experimentally the effects of foam filling on the compressive response of hexagonal cell aluminum honeycombs under axial compression and found that the mean crushing strength and energy absorption were enhanced up to 300%. Subsequently, Mahmoudabadi and Sadighi [2011] developed a theoretical model to determine the mean crushing strength of foam-filled honeycombs under both quasistatic and dynamic compression, whilst Burlayenko and Sadowski [2010] predicted the effective elastic properties of such foam-filled honeycombs using FE analysis.

Based upon FE simulations, Vaziri et al. [2006] assessed the mechanical properties of metallic sandwich plates having corrugated cores and square honeycomb cores, both filled with polymer foam (Divinycell). Whilst the foam-filled cores showed greater out-of-plane shear strength, they were not comparable to the equivalent unfilled cores in terms of compression strength; further, under quasistatic punch loads and impulsive loads, the foam-filled cores only exhibited comparable structural performance in resisting deformation to the unfilled ones with equal mass. Through hybridization of glass and carbon fibers as well as foam filling, Zhang et al. [2013] attempted to improve the bending strength and energy absorption of corrugated sandwich composite structures. Due to the better support of the web by the filling foam, the peak load was increased, delaying debonding of the core and face sheets, and thus core failure. However, the improvement in crashworthiness was not significant as the foam used was relatively weak (low density).

Yoo et al. [2010] tested foam-filled composite egg-box sandwich panels under compression and found that this construction showed good energy absorption capacity with stable collapse response. Further, the filling with low density foams led to the best energy absorption performance of the sandwich. An integrated orthogrid stiffened syntactic foam core was investigated with both low velocity impact tests and compression after impact (CAI) tests [Li and Muthyala 2008]. The integrated core exhibited enhanced impact energy absorption and positive composite action with higher CAI strength.

Recently, with the goal of combining the desirable attributes of stochastic foams and lattice truss structures, Ostos et al. [2012] inserted polyurethane foams with submillimeter pores into the centimeter-scale interstices of low-density polymer lattices and assessed the concept in terms of quasistatic compressive response. It was demonstrated that the filling of even a weak foam could double the crushing strength of the lattice. Based upon X-ray computed tomography and FE analysis, the elevation was attributed to the lateral support of the strut members against buckling provided by the surrounding foam.

Existing studies regarding the effects of foam filling upon the mechanical performance of sandwich constructions focused mainly on polymer foams. Further, the unfilled sandwiches considered were constructed mainly with nonmetallic materials such as polymer or fiber-reinforced composites. One notable exception was the work of Yan et al. [2013] who inserted close-celled aluminum foams into the interstices of corrugated sandwich panels made of stainless steel and assessed the performance of the sandwich under quasistatic compression. It was demonstrated that, relative to empty corrugated sandwiches, foam filling could increase significantly not only the crushing strength but also the specific energy absorption. It was further shown that the core web was considerably stabilized by the filling foam against lateral deflection. In particular, the elasto-plastic buckling wavelength was significantly reduced and the transition from axial deformation to bending of the core web was much delayed, both contributing to enhanced strength and energy adsorption. As a result, the post-yielding response of the foam-filled sandwich was altered in such a way that crushing occurred at a nearly constant stress, consistent with the finding of Ostos et al. [2012] for polymer lattice structures filled with polymer foams.

1.2. Scope of present study. Built upon the mainly experimental work of Yan et al. [2013], the present investigation aimed to model numerically the quasistatic out-of-plane compressive response of metallic corrugated sandwich panels filled with close-celled aluminum foams, and then use the numerical models to explore the underlying physical mechanisms and construct the collapse mechanism maps. After specifying the problem in Section 2, FE models for both empty and foam-filled corrugated plates were

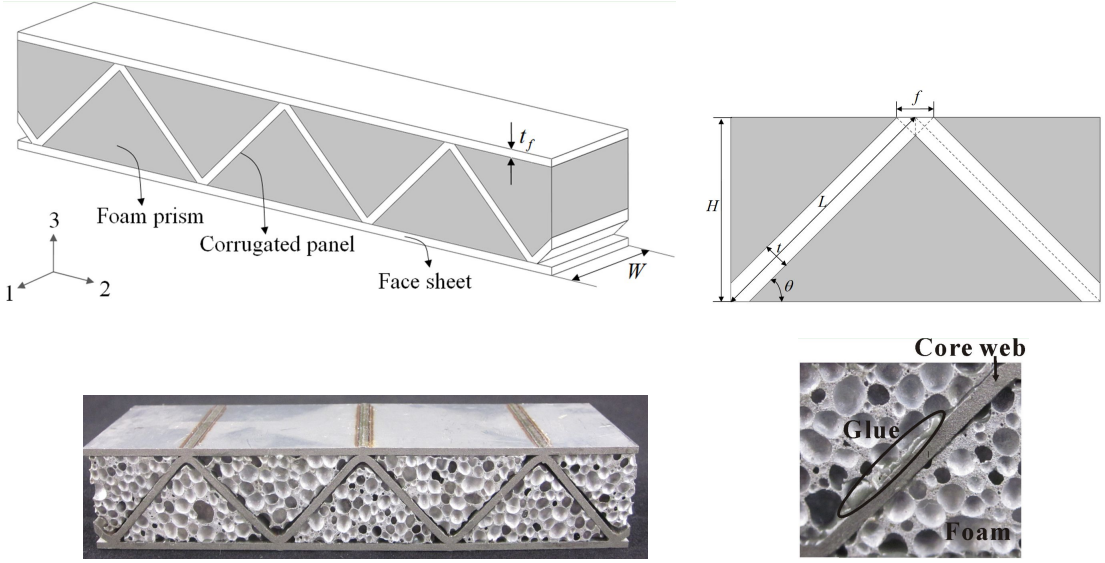


Figure 1. Schematic representation of foam-filled corrugated sandwich plate (top left), unit cell (top right), typical as-fabricated sandwich (lower left), and interface between foam and core web showing good bonding condition (lower right).

constructed in Section 3, and the validity of FE model predictions was checked against experimental measurements. In Section 4, the effects of key geometrical and material parameters were systematically investigated and the physical mechanisms underlying the strengthening effect of foam filling explored. Further, based upon the different deformation modes of post-buckling identified, collapse mechanism maps were constructed. Finally, in Section 5, the strength and energy absorption capabilities of the foam-filled corrugated plates were compared with competing lightweight structures.

2. Specification of foam-filled sandwich plates

The foam-filled corrugated sandwich plate and the corresponding unit cell were shown schematically in Figure 1 (top left and right, respectively). The sandwich structure was characterized by inclination angle θ , core height H , face sheet thickness t_f , width W , strut (core web) thickness t , length L , and foam relative density $\bar{\rho}_f$ (nondimensional) or density ρ_f (dimensional). For convenience, let the density ratio $\bar{\rho}$ be defined as the ratio of the average density ρ_c of the foam-filled corrugated core to the density ρ_s of the strut material as

$$\bar{\rho} \equiv \rho_c / \rho_s = \lambda + (1 - \lambda) \rho_f / \rho_s, \quad (1)$$

where λ denoted the volume fraction of the core occupied by the solid struts. To calculate λ , it was assumed that an overlap region was formed at the joint of two inclined struts, as illustrated in Figure 1 (top right). Accordingly, the height and width of the half unit cell were $H = L \sin \theta$ and $B = L \cos \theta$, whilst the width of the overlap region was $f = t / \sin \theta$. The overlap area may thence be expressed as

$$A_{\text{overlap}} = \frac{t^2}{2 \sin 2\theta}.$$

With the area occupied by the overlap accounted for, one arrived at

$$\lambda = \frac{tL - A_{\text{overlap}}}{HB} = \frac{t/L}{\sin 2\theta} \left(2 - \frac{t/L}{\sin 2\theta} \right). \quad (2)$$

Previously, by considering the area occupied by each strut separately (i.e., ignoring the overlap of [Figure 1](#), top right), Vaziri et al. [2006] obtained an alternative expression as

$$\lambda = \frac{t/L}{t/L + \frac{1}{2} \sin 2\theta}. \quad (3)$$

For illustration, consider the case of $\theta = 45^\circ$ and $\rho_f = 648 \text{ kg/m}^3$. The two predictions were nearly identical for small slenderness ($t/L < 0.05$), but diverged at larger values ($t/L > 0.05$). Further, (2) gave predictions closer to those measured experimentally (mass contribution of epoxy glue ignored; see discussion below). Henceforth, (2) together with (1) were employed in the present study to calculate ρ_c and $\bar{\rho}$.

The fabrication procedures for all-metallic corrugate-cored sandwich plates filled with aluminum foams were straightforward. Corrugated plates were firstly fabricated via a folding operation. Empty (unfilled) corrugated sandwich plates were then assembled by laser welding the face sheets to the folded plates. Subsequently, triangular foam prisms cut by electrodischarge machining (EDM) from close-celled aluminum foam sheet were inserted into the interstices of the empty sandwich and fixed using epoxy glue. As impaired bonding condition between the foam and the face sheets as well as the folded plates may reduce the mechanical performance of the foam-filled sandwiches, the interfaces were treated carefully to minimize the clearance before epoxy glue was applied to fill the gaps.

In the present study, both the face sheets and the corrugated plates were made of 304 stainless steel with density $\rho_s = 7900 \text{ kg/m}^3$. The aluminum foam with closed cells was fabricated via the foaming route, similar to the commercial Alporas foam that had been extensively studied. Aluminum foams with two different relative densities were used, called here as foam I and foam II. Foam I had a relatively high density of $\rho_f = 648 \text{ kg/m}^3$ (porosity 0.76) whilst foam II had a relatively low density of $\rho_f = 324 \text{ kg/m}^3$ (porosity 0.88).

Three kinds of empty sandwich plates having different strut thicknesses ($t = 0.41 \text{ mm}$, 0.82 mm and 1.42 mm), with the remaining morphological parameters fixed at $\theta = 45^\circ$, $H = 17 \text{ mm}$, $t_f = 1.42 \text{ mm}$ and $W = 20 \text{ mm}$, were fabricated. Correspondingly, foam-filled sandwiches using both foam I and foam II were fabricated. A typical foam-filled sandwich plate was shown in [Figure 1](#) (bottom left). The interface between the foam and the core web was highlighted in [Figure 1](#) (bottom right), indicating that good bonding condition had been achieved. Both the empty and foam-filled sandwich plates were tested under out-of-plane (direction-3 in [Figure 1](#), top left) compression, with constant displacement loading rate of 10^{-4} s^{-1} (corresponding to a loading speed of 0.12 mm/min) at room temperature. The measured results were used later to compare with analytical predictions for the compressive strength of foam-filled sandwiches and to validate FE simulations. More details of the experiments were referred to Yan et al. [2013], who also provided preliminary FE simulation results.

3. Finite element modeling

3.1. Constitutive model and material specifications. The parent material (as-brazed 304 stainless steel) of the core webs and the face sheets was modeled as an isotropic and homogeneous elastic-plastic solid of elastic modulus $E_s = 210$ GPa, Poison ratio $\nu = 0.3$, yielding stress $\sigma_Y = 210$ MPa, and linear hardening with tangent modulus $E_t \equiv d\sigma/d\epsilon \approx 2.1$ GPa. The classical theory of flow plasticity based on the von Mises yield surface and isotropic hardening was applied, whilst the quasistatic tensile stress versus strain curve of 304 stainless steel was taken directly from [Côté et al. 2006]. The steel was assumed sufficiently ductile to sustain large strains without fracture, as confirmed by experiments.

The isotropic phenomenological constitutive model of Deshpande and Fleck [2000] for metallic foams was employed to model the aluminum foam insertions. With isotropic hardening assumed, the yield surface of the foam was defined as

$$\hat{\sigma} - Y = 0 \quad (4)$$

where Y represented the size of the yield ellipse, and $\hat{\sigma}$ was the equivalent stress given by

$$\hat{\sigma}^2 \equiv \frac{1}{1 + (\beta/3)^2} [\sigma_e^2 + \beta^2 \sigma_m^2], \quad (5)$$

$$Y = \sigma_e \sqrt{1 + \left(\frac{\beta}{3}\right)^2}. \quad (6)$$

Here, $\sigma_e = \sqrt{3s_{ij}s_{ij}/2}$ was the von Mises equivalent stress, $\sigma_m \equiv \sigma_{kk}/3$ was the mean stress, s_{ij} was the deviatoric stress, whilst β was a material parameter representing the ratio of deviatoric strength to hydrostatic strength. The normalization factor on the right hand side of (5) ensured that $\hat{\sigma}$ was equal to the stress in a uniaxial tension or compression test. With the normality of plastic flow assumed, the ‘‘plastic Poisson’s ratio’’ $\nu_p = -\dot{\epsilon}_{22}^p/\dot{\epsilon}_{11}^p$ for uniaxial compression in direction 1 was given by

$$\nu_p = \frac{1/2 - (\beta/3)^2}{1 + (\beta/3)^2}, \quad (7)$$

from which

$$\beta = \frac{3}{\sqrt{2}} \sqrt{\frac{1 - 2\nu_p}{1 + \nu_p}}. \quad (8)$$

Figure 2 presented the experimentally measured uniaxial compressive stress versus strain curves of foam I (porosity 0.76) and foam II (porosity 0.88). For foam I, the plastic Poisson ratio ν_p was measured to be 0.21, thus $\beta = 1.47$. Other parameters were also measured for foam I, as: $E_f = 2.61$ GPa, $\nu_f = 0.3$, and $\sigma_{\text{plateau}} \approx 14.5$ MPa. For foam II, $\nu_p \approx 0$ (and hence $\beta \approx 2.12$), $E_f = 157$ MPa, $\nu_f = 0.3$, and $\sigma_{\text{plateau}} \approx 3.0$ MPa. Note that, due to alloying, foam I exhibited somewhat brittleness as a result of successive fracturing of cell membranes. This led to the wiggling of the stress versus strain curve once initial yielding was initiated, yet a long plateau regime typical for aluminum foams was still present (Figure 2). For the purpose of FE simulation with the commercial code Abaqus, the stress versus strain curve of foam I was smoothed as illustrated in Figure 2.

For both foam I and foam II, the average cell size was approximately 2.5 mm, allowing at least seven cells along each leading dimension of the foam-filled sandwich core. Consequently, it was considered

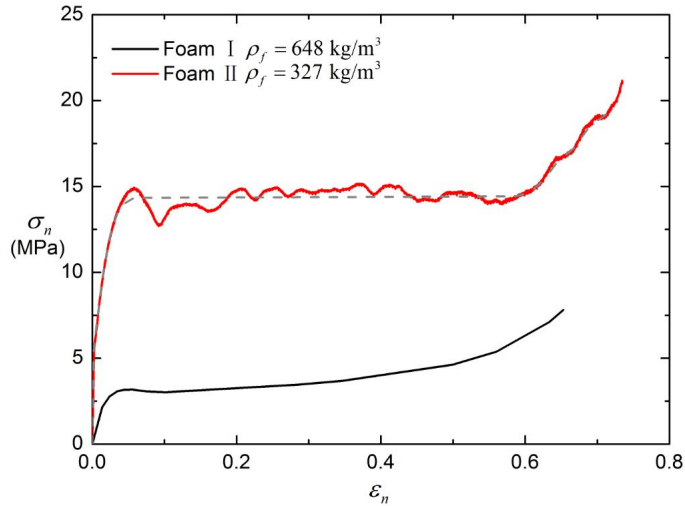


Figure 2. Compressive stress versus strain curve of close-celled aluminum foams measured at strain rate of 10^{-4} s^{-1} .

reasonable to use the phenomenological constitutive model to describe the macroscopic mechanical properties of the filling foam.

3.2. Finite element model. Experimentally it was observed that, at large nominal compressive strains (direction 3; see Figure 1, top right), partial extrusion of the foam insertions occurred along direction-1 and the foam-filled sandwich plate exhibited slight transverse buckling along the same direction. Consequently, three-dimensional (3D) FE models were developed using ABAQUS/Explicit (NLGEOM=YES in ABAQUS notation), with eight-node linear brick elements having reduced integration (C3D8R) adopted. Whilst the element size was set at about $H/50$ for the whole model, it was about $t/6$ for the core web along the thickness direction. It was established that the accuracy of the calculations was not improved appreciably with additional mesh refinements.

Geometrical imperfections were inevitable in corrugate-cored sandwich structures. However, for the present foam-filled sandwich plates, it was found that good agreement between experimentally measured uniaxial compressive stress versus strain curves and those predicted using FE simulations was achieved without considering any initial geometrical imperfections (Figure 3). Therefore the influence of geometrical imperfections was neglected in the present study.

As previously mentioned, to fabricate the sandwich plates, a thin film of epoxy glue was used to bond the foam prisms to the core webs and face sheets. To investigate the influence of interfacial bonding between stainless steel and aluminum foam on peak load and energy absorption, Yan et al. [2013] carried out FE simulations for foam-filled sandwich panel having both perfectly bonded and unbonded interfaces. It was demonstrated that the simulated results with perfect bonding matched better with experimental measurements, suggesting that the use of epoxy glue provided good bonding between aluminum foam and stainless steel (see Figure 1, bottom right). Although debonding was indeed observed when large plastic deformation occurred, all subsequent FE simulations were based on perfect bonded interfaces as the present mechanism analysis aimed to focus on the early stage of deformation (compressive strain not

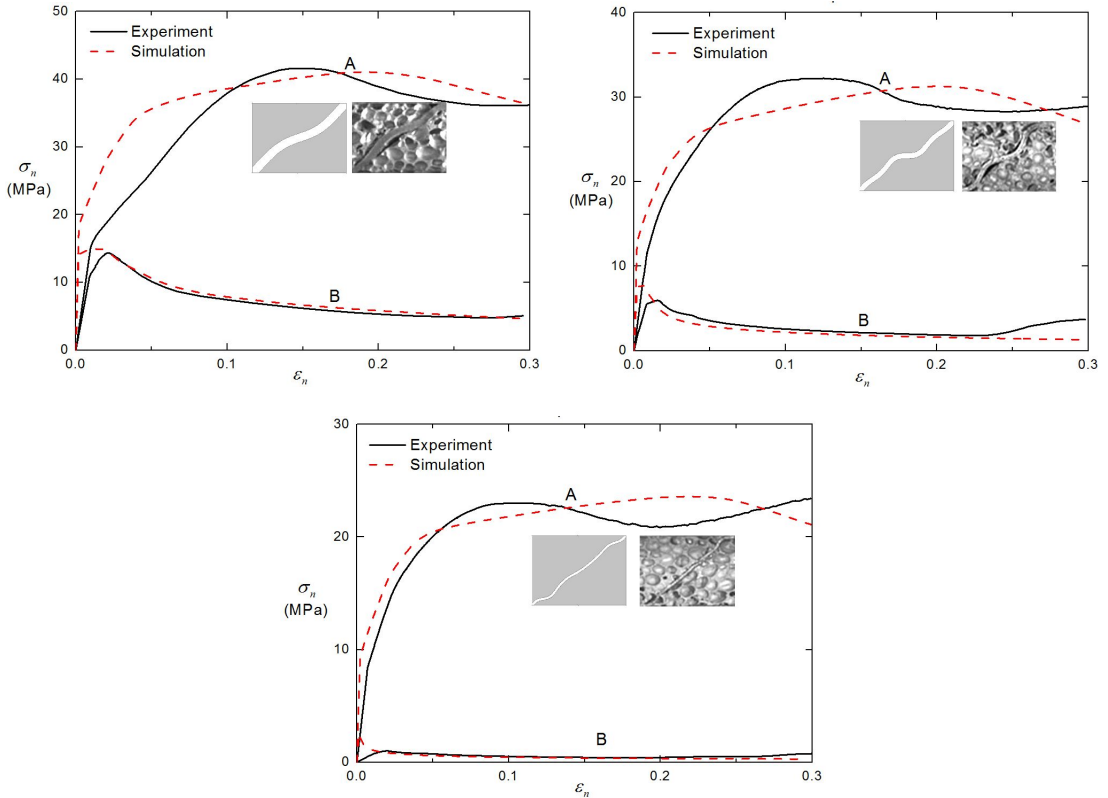


Figure 3. Comparison of FE simulated nominal compressive stress versus nominal compressive strain curves with those measured: specimen 1 ($t/L = 0.059$) (top left); specimen 2 ($t/L = 0.034$) (top right); specimen 3 ($t/L = 0.017$) (bottom). Both inserted photo and FE simulation of deformation mode correspond to $\epsilon_n = 0.30$. Curve A denoted compressive response of foam-filled core, whilst curve B denoted the corresponding empty core, with inclination angle fixed at $\theta = 45^\circ$ and foam I used as insertions.

exceeding 0.30). In the FE model, the perfectly bonded interfaces between foam prisms and struts (as well as face sheets) were modeled using the Tie option provided in ABAQUS.

To simplify the calculations, only half of the unit cell was employed as the representative volume element (RVE), with symmetric boundary conditions applied on the two edge-planes parallel to direction-3, as shown in Figure 4 (left). Both the top and bottom face sheets were set as rigid surfaces. The bottom face was fixed while the top face was displaced in direction-3 only, with a constant loading rate of 1.0 s^{-1} . The loading rate was sufficiently low to ensure that the simulated crushing response was quasistatic. The absence of significant oscillations in the resulting load versus deflection curves and the small kinetic energy acquired by the sandwich core (less than 5% of the strain energy) confirmed the validity of the approach, as suggested in the ABAQUS documentation [DSSC 2007]. Further, the lack of symmetry about the centroid of either the empty or foam-filled core was sufficient to cause a preferential buckling direction of the sandwich. Finally, as shown in Figure 4 (right), additional calculations with more unit

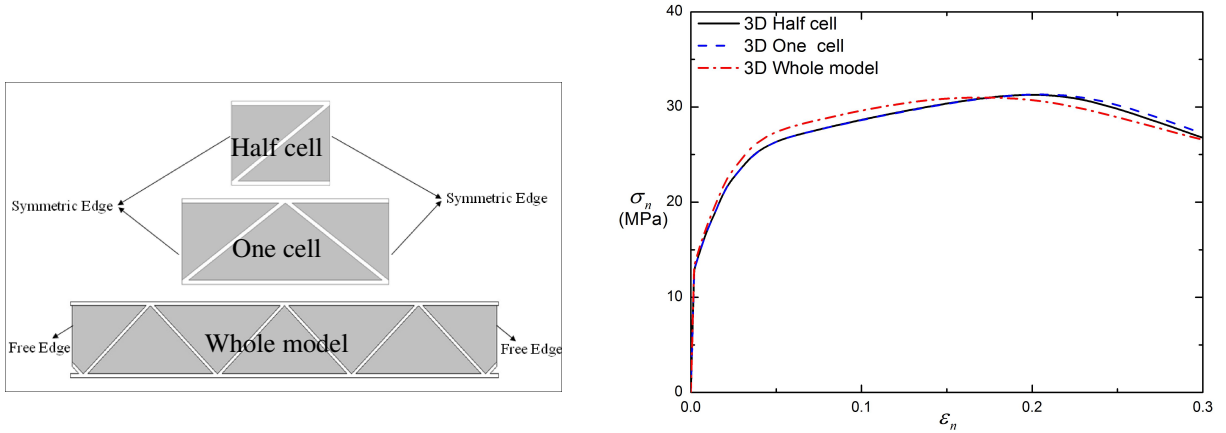


Figure 4. FE model (left): half cell and one cell with symmetric edges, as well as whole model with free edges (just like the specimen shown in Figure 1, bottom left). On right: influence of cell number upon simulated compressive response of a foam-filled corrugated sandwich with $t/L = 0.0341$, $W/H = 1$, $\theta = 45^\circ$, and foam I as the fillers.

t/L	foam I-filled core		Empty corrugated core		
	Test (MPa)	FE (MPa)	Test (MPa)	FE (MPa)	Theory [†] (MPa)
0.017	23.02	23.60	1.04	3.56	3.69
0.034	32.20	31.26	5.94	8.02	7.37
0.059	41.61	41.07	14.38	14.94	13.85

Table 1. Comparison of FE predictions with test results of compressive strength for both empty and foam I-filled cores with $\theta = 45^\circ$ and varying core web slenderness ratios. [†]Analytical prediction for buckling of empty corrugated core was outlined in the Appendix.

cells were performed, giving nearly identical results as those obtained by using the RVE model. Thus, in all subsequent FE calculations, the half cell model with symmetric edges was employed as the RVE.

3.3. Validation against experimental measurement. Experimental measurements under quasistatic out-of-plane compression were carried out following Yan et al. [2013]. Table 1 compared the FE simulation results with experimental measurements for the compressive strength (peak compressive stress) of both empty and foam I-filled corrugated cores, with the inclination angle fixed at $\theta = 45^\circ$ and the strut slenderness ratio t/L varied as 0.059, 0.034 and 0.017 (i.e., specimen 1, specimen 2 and specimen 3 in Figure 3). The corresponding stress versus strain curves were presented in Figure 3, together with the FE simulated and experimentally measured deformation modes of the foam-filled core at $\epsilon_n = 0.30$.

Existing studies [Côté et al. 2006; Yan et al. 2013] suggested that the collapse of empty corrugated plates under out-of-plane compression was governed by Euler buckling for thin plates and global plastic

buckling for thick plates. In contrast, the foam-filled corrugated plates deformed by forming more plastic hinges and exhibited no obvious softening after the peak stress was reached (Figure 3), increasing significantly its specific strength and energy absorption, as previously mentioned by Yan et al. [2013].

For the peak compressive stress, the results of Table 1 demonstrated that, overall, good agreement was achieved between FE simulation and measurement. In particular, the errors of the peak stress between FE simulation and measurement for foam-filled corrugated cores were only 1.3% ~ 2.9%. There was also good agreement between FE simulated and experimentally measured stress versus strain curves (Figure 3). Further, the deformation and collapsing modes of the foam-filled cores were accurately captured by the FE simulation. The results shown above served to confirm the fidelity of the FE simulations for the foam-filled corrugated cores. As geometrical imperfections were neglected in the present FE modeling, the results of Table 1 and Figure 3 also indicated that the compressive properties of foam-filled corrugated cores were insensitive to the presence of geometrical imperfections.

For the empty corrugated cores, however, the discrepancy between simulation and measurement increased as the core web thickness was reduced; see Table 1. This was understandable, as the compressive properties of empty corrugated cores were sensitive to the presence of geometrical imperfections in particular when the core web was relatively thin. As previously mentioned, the present FE simulations ignored the effects of geometrical imperfections whilst, in reality, such imperfections were inevitable during the fabrication of the corrugated core.

Under the assumption that the core webs were slender, its out-of-plane compressive strength may be analytically predicted, as demonstrated in the Appendix. For the present empty corrugated cores considered, the analytically predicted compressive strength was listed in Table 1. Whilst the analytical prediction overestimated the experimentally measured compressive strength, it agreed quite well with that calculated numerically. This was attributed to the fact that both the theory and FE simulation ignored the effects of geometrical imperfections.

Finally, it should be mentioned that the present FE simulations were carried out up to the nominal compressive strain of 0.30, beyond which the discrepancy between the simulation and the experiment notably increased. This was because that, at large strains, the large rotation of the plastic hinges caused foam/strut interfacial debonding and the foam insertions began to be squeezed out (along direction-1) of the interstices of the corrugated core.

4. Results and discussion

In this section, using the experimentally validated FE methodology, we carried out a systematic study over a wide range of corrugation configurations, characterized by $0.005 \leq t/L \leq 0.3$, $35^\circ \leq \theta \leq 65^\circ$, and $W/H = 1$. For each configuration, three different kinds of sandwich panels having foam I-filled, foam II-filled, and empty corrugated cores were considered. The aim was to explore in detail the physical mechanisms underlying the strengthening effect of foam insertions and construct the collapse mechanisms map for the foam-filled cores.

4.1. Strengthening effects of foam insertions.

4.1.1. Crushing response and strengthening mechanisms. Details concerning the FE calculated compressive response of a typical foam-filled corrugated core (specimen 2), with inclination angle $\theta = 45^\circ$,

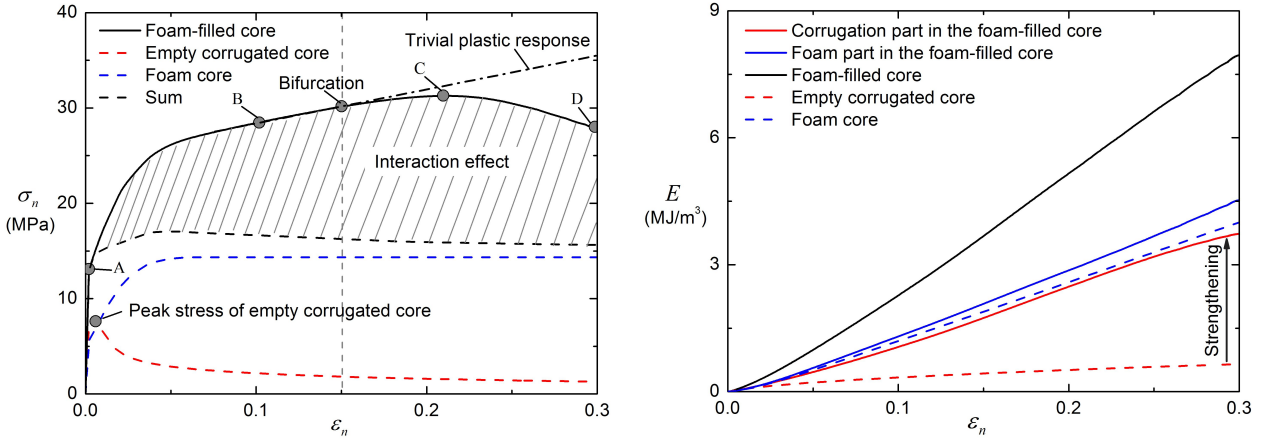


Figure 5. Finite element simulation results: nominal compressive stress versus nominal compressive strain curves (left) and energy absorbed by foam-filled core and its constituents plotted as functions of nominal compressive strain (right), with $\theta = 45^\circ$, $t/L = 0.034$ and foam I insertions.

slenderness ratio $t/L = 0.034$ and foam I insertions, were presented in Figure 5, which had all the common features of foam-filled cores under quasistatic out-of-plane compression.

Figure 5 (left) presented the nominal compressive stress (σ_n) versus nominal compressive strain (ϵ_n) curve up to $\epsilon_n = 0.30$. The red and blue dash lines represented separately the crushing responses of the empty core and foam I, the black dash line was the sum of the two, whilst the black solid line denoted the response of the foam-filled core as a whole. The interaction effect (represented by the shaded area in Figure 5, left) between the filling foam and the core web was strong, not only enhancing significantly the peak stress but also reduced considerably core softening once the peak stress was reached.

It is seen from Figure 5 (left) that the nominal compressive stress of the foam-filled core increased linearly with increasing strain till the first inflection point A ($\epsilon_n \approx 0.0012$), which signified core yielding. Subsequently, the curve entered a nonlinear region, due to material nonlinearity of both the strut material and foam I. In particular, the core behaved in a stable manner once the stress plateau of the foam insertions was reached, exhibiting nearly linear plastic hardening over a large range of ϵ_n as a result of the plastic hardening of 304 stainless steel. As the strain was further increased to $\epsilon_n \approx 0.15$, bifurcation was observed at the intersection between the lines of extended trivial plastic response and the actual response. Note from Figure 5 (left) that after the nonlinearity of the stress versus strain curve due to material nonlinearity, there was a linear segment (within the range of compressive strain 0.07–0.15) of the curve before strut buckling occurred. This linear response and its extension (dashed line in Figure 5, left) was defined here as the trivial plastic response, just as the elastic trivial response shown in Figure 7 of [Wilbert et al. 2011]. At the bifurcation point marked on the curve, the strut started to buckle and hence the actual stress strain curve deviated from such trivial response as shown in Figure 5 (left). Subsequently, the tangent modulus started to drop and the nonlinearity at kinematic levels showed up as plastic bending was initiated in the struts. With further compression, the extended bending deformation led to strut collapse at which point

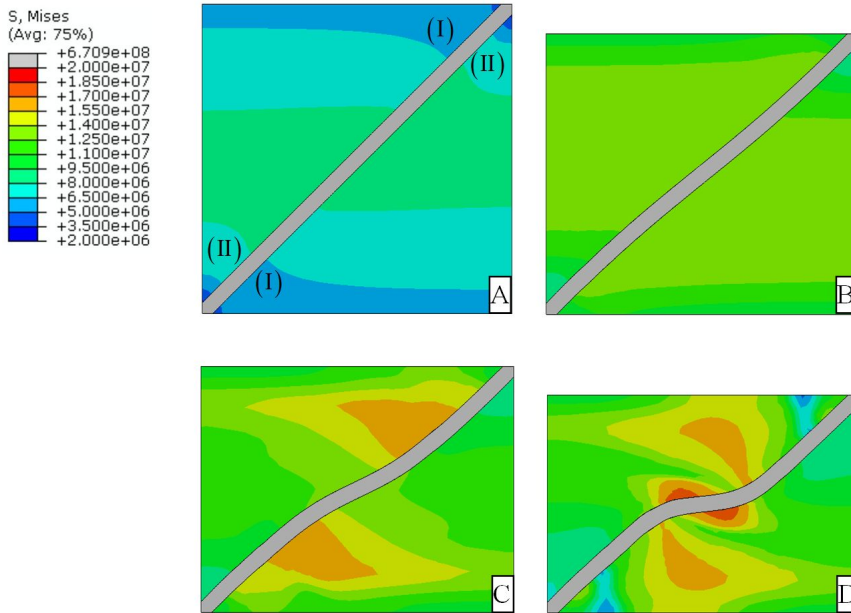


Figure 6. Contours of von Mises stress in foam insertions at specific strains corresponding to the four specified points of Figure 5 (left).

the peak stress of the core was reached. In comparison with the empty core, the peak stress corresponding to point C of Figure 5 (left) was considerably delayed due mainly to foam/strut interaction.

To explore further the strengthening effect of foam insertions, Figure 4 (right) presented the internal energy (plastic dissipative energy and strain energy) for each constituting element of the foam-filled core; corresponding results for the empty core and the foam itself were also presented. The internal energy, defined here as the energy absorbed by each constituting element, was calculated by integrating stress with respect to strain (up to overall nominal compressive strain of 0.3), which were extracted from the post-processing of ABAQUS. The kinematic energy was neglected as the loading rate was sufficiently low. From Figure 5 (right) it was clear that the strengthening was mainly attributed to the dramatic enhancement of the strut, as its internal energy per unit volume was greatly enhanced relative to that in the empty core. Simultaneously, the energy per unit volume of the foam insertions was also increased, although not as dramatic.

For the foam insertions, Figure 6 presented a set of contours of the von Mises equivalent stress in the central cross-section ($x_1 = W/2$; Figure 1, top left) of the RVE for selected compressive strains as marked in Figure 5 (top left). During the early stage of compression (contour A), the main regimes of the equivalent stress originated from the core center, and expanded gradually to the top and bottom faces with increasing compression. At $\epsilon_n = 0.10$ (contour B), the distribution of the equivalent stress was nearly layer-wise homogeneous, averaging to about 14.5 MPa, which equaled approximately the plateau stress of foam I (Figure 2). This implied that the foam deformation was dominated by the compressive stress along the loading direction (direction-3), resulting in almost the same response as that of uniaxially compressed foam I (Figure 2). However, under out-of-plane compression, the stress

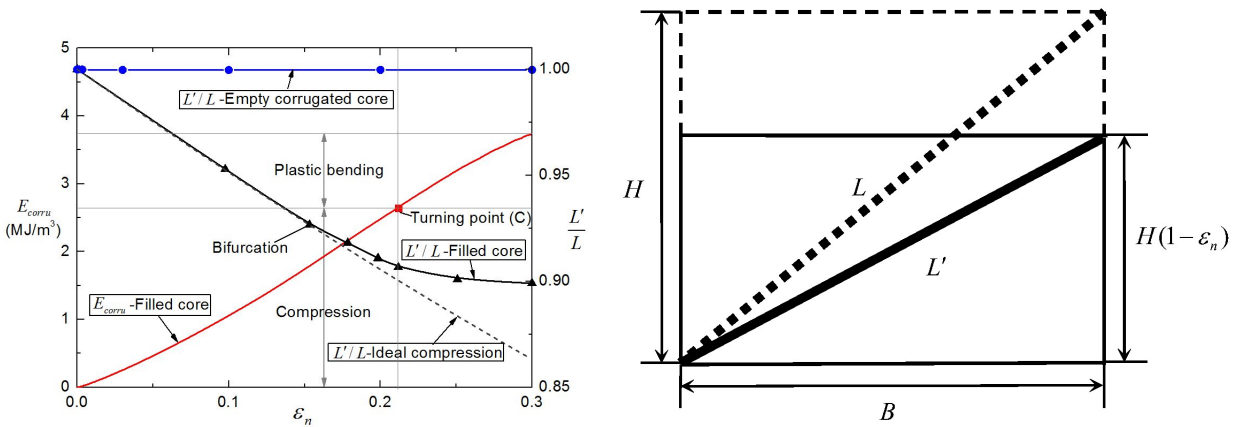


Figure 7. Left: energy absorbed by corrugated plate and length reduction of its middle line plotted as functions of nominal compressive strain, with $\theta = 45^\circ$, $t/L = 0.034$, and foam I insertions. Red square point defined as the “turning point” referred to the peak stress of foam-filled corrugated plates. Right: Sketch of an inclined strut experiencing only axial compression: dotted and solid bold lines denoted separately initial and deformed middle lines of the strut.

state in the foam insertion was asymmetric around the two ends of the corrugated plate, as shown in contours A and B. Let the foam region adjacent to the face sheet be defined as region I and the others be defined as region II, as shown in contour A of Figure 6. Initially, the stressing and foam densification in region II was more intense than that in region I. As the compressive strain was increased, region I was gradually enlarged, as shown in contour B. That the stress in region I was greater than that in region II caused a rotational moment on the corrugated plate, inducing odd-symmetrical bending (see discussion later concerning Figure 20). As a result of the bending deformation, severe stress localization occurred, inducing complicated combination of compression, tension, and shear as well as localized densification in the foam surrounding the bent corrugated plate, as illustrated in contours C and D. Correspondingly, the amount of energy absorbed by the foam insertion noticeably increased.

Note that the deformation of the corrugated plate shown in contour D of Figure 6 was somewhat different from that in Figure 3 (top right) at the same strain level of $\epsilon_n = 0.30$. This was expected, as for the present 3D sandwich configurations with finite width W (Figure 1), the constraints provided by the foam insertions on the corrugated plates were not homogeneous along the direction-1, relatively weak closer the free boundaries of the sandwich. Unless otherwise stated, the deformation and collapse modes discussed latter were all referred to the central cross-section of the RVE.

Consider again specimen 2. Let E_{corr_u} denote the energy absorption of the corrugated plate in the foam-filled core per unit volume and L'/L denote the normalized length change of the middle line (the reference line) of the corrugated plate, representing the deformed state of the latter. Figure 7 (left) plotted separately E_{corr_u} and L'/L as functions of the compressive strain ϵ_n . By assuming that the strut experienced only axial compressive deformation (i.e., length change due to bending excluded) as shown in Figure 7 (right), the normalized length of the middle line of the strut after deformation may be

expressed as

$$\frac{L'}{L} = \sqrt{\frac{H^2(1 - \epsilon_n)^2 + B^2}{L^2}} = \sqrt{\sin^2 \theta (1 - \epsilon_n)^2 + \cos^2 \theta}. \quad (9)$$

For comparison, the prediction from the above equation was also plotted (dashed line) in [Figure 7](#). The actual length change of the corrugated plate coincided with that calculated with [Equation \(9\)](#) until the bifurcation point was reached (see also [Figure 5](#) (left)). This implied that, before bifurcation occurred, the corrugated plate experienced only axial compression along its middle axial line. However, after the bifurcation, the corrugated plate lost stability and collapsed, with its deformation gradually shifting from axial compression to bending. Correspondingly, the rate at which its length decreased slowed down ([Figure 7](#), left). After the turning point corresponding to the peak stress of the foam-filled core (point C in [Figure 7](#), left), the length of the corrugated plate was almost unchanged, indicating that its deformation was now dominated by bending. In comparison, the length of the corrugated plate in an empty (unfilled) sandwich remained unchanged, as bending rather than axial compression dominated its deformation under out-of-plane compression.

Before the turning point was reached, the energy absorbed by the corrugated plate, E_{corr} , was dominated by axial compression, exhibiting a slightly accelerated growth as the nominal compressive strain ϵ_n was increased ([Figure 7](#)). Beyond the turning point, the energy absorption was mainly attributed to plate bending, with decelerated growth. In other words, for foam-filled cores, whilst the deformation of the corrugated plate was dominated by axial compression during the pre-buckling stage (before the peak stress was reached), bending deformation played the dominant role in the post-buckling regime. Further, with aluminum foam insertions, not only was the buckling of the corrugated plate greatly delayed, leading to significantly enhanced peak stress of foam-filled cores, but also much less obvious softening in the post-buckling regime. Similar results were recently observed experimentally in polymer lattice structures filled with polyurethane foams [[Ostos et al. 2012](#)].

4.1.2. Effect of inclination angle. [Figure 8](#) presented the predicted overall compressive responses of both foam-filled and empty corrugated cores for selected inclination angles of θ and fixed core web slenderness ratio of $t/L = 0.02$. In general, as θ was increased, both the strength and energy absorption of the sandwich core increased. Further, the stress versus strain curves (up to $\epsilon_n = 0.30$) of the foam-filled cores with smaller inclination angles were smoother. For small inclination angles especially when $\theta \leq 35^\circ$, the contribution by the core web to load bearing was relatively small in comparison with that by the foam insertions; therefore, the foam insertions dominated the load bearing, leading to smoother compressive curves of the sandwich cores ([Figure 8](#)). Irrespective of the inclination angle, the critical strain at which the core web collapsed (plastically buckled; corresponding to the peak stress of [Figure 8](#)) was remarkably delayed with foam filling, particularly so if the foam relative density was large (e.g., foam I). In comparison, in the absence of foam filling, the core web easily collapsed with a tiny critical strain (ranging from 0.002 to 0.004; [Figure 8](#), bottom).

With the core web slenderness ratio fixed at $t/L = 0.02$, the results of [Figure 8](#) suggested that the compressive properties of corrugated cores filled with either foam I or foam II were considerably superior to those of empty cores. Further, the filling of a denser foam (i.e., foam I) led to larger specific strength and energy absorption per mass, almost twice those obtained with foam II insertions.

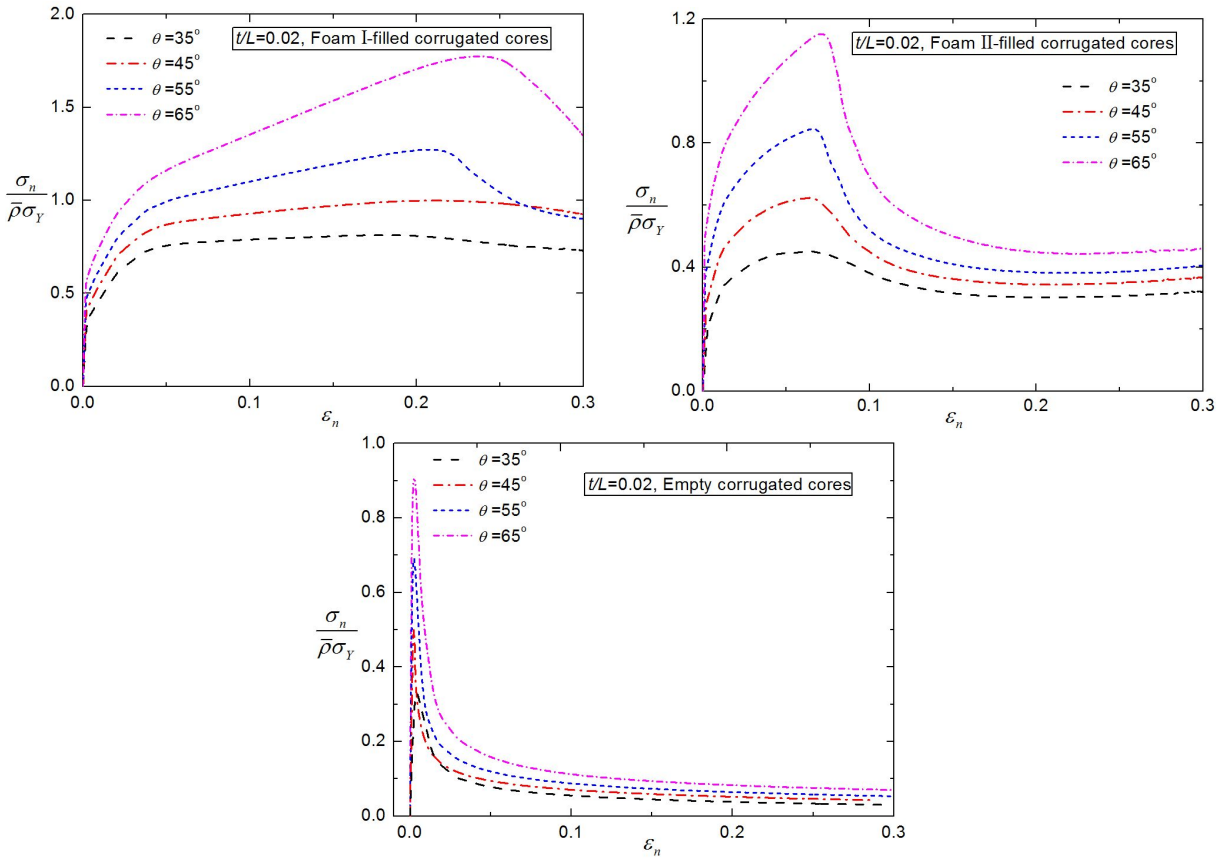


Figure 8. Normalized nominal compressive stress versus nominal compressive strain curves for selected inclination angles: foam I-filled cores (top left); foam II-filled cores (top right); empty cores (bottom). Core web slenderness ratio fixed at $t/L = 0.02$.

To explore further the strengthening mechanisms of foam insertions, the effects of inclination angle on energy absorption per unit mass (up to $\epsilon_n = 0.30$) were presented in Figure 9 (top left) for both empty and foam-filled cores, in Figure 9 (top right) for corrugated plates only, and in Figure 9 (bottom) for foam insertions only. As reference, the corresponding results for foam I and foam II were also plotted in Figure 9 (bottom). With foam filling, not only was the energy absorption capability of the core webs significantly enhanced, but also was the energy absorption capability of the foam itself enhanced (due to complex stressing); see Figure 9 (top right and bottom). Moreover, as θ was increased, whilst the amount of energy absorbed by the core webs in the foam-filled core increased appreciably, that absorbed by the foam insertions remained more or less unchanged.

Figure 10 plotted separately the normalized length reduction and maximum lateral deflection of the core web (up to $\epsilon_n = 0.30$) as functions of the inclination angle for both foam-filled and empty corrugated cores having fixed core web slenderness ratio of $t/L = 0.02$. Again, for empty cores, the length of the core web remained almost unchanged ($\delta/L = 0$; $\delta \equiv L - L'$ denoted the length reduction) as θ was varied, with deformation dominated by plate bending. For foam-filled cores, whilst increasing θ led to

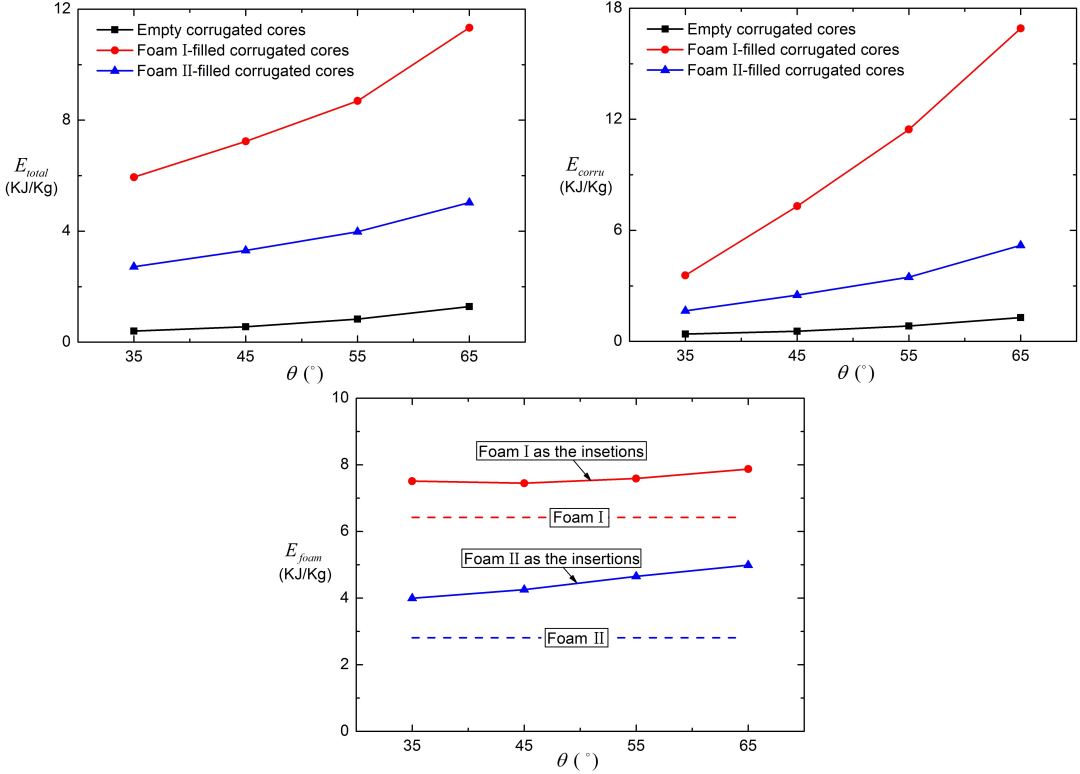


Figure 9. Effect of inclination angle on energy absorption per unit mass (up to nominal compressive strain of 0.30) for empty and foam-filled cores (top left), corrugated plates only in empty and foam-filled cores (top right) and foam insertions only in foam-filled cores (bottom), with corresponding results for foam I and foam II under out-of-plane compression also plotted as reference. Core web slenderness ratio fixed at $t/L = 0.02$.

increasing axial compression (length reduction) of the core web, the length reduction was more severe in the presence of denser foams. Although the maximum lateral deflection of the core web also increased with increasing θ , the variation trend was opposite to that of its length reduction: for a fixed inclination angle, the core web in an empty core exhibited the largest deflection whilst that in foam I-filled core had the least deflection; see Figure 10 (right).

4.1.3. Effect of core web slenderness ratio. Let σ_p denote the peak compressive stress and E denote the energy absorption per unit volume of the RVE up to $\epsilon_n = 0.30$. For both foam-filled and empty corrugated cores, Figure 11 (left) plotted the specific strength, $\sigma_p/(\bar{\rho}\sigma_Y)$, as a function of slenderness ratio t/L , with the inclination angle fixed at $\theta = 45^\circ$. Corresponding results for specific energy absorption, $E/(0.3\bar{\rho}\sigma_Y)$, were presented in Figure 11 (right). Although not shown here, similar results for other inclination angles were also obtained.

With increasing t/L , both the specific strength and specific energy absorption increased, and the increase was more significant at large t/L values with or without foam filling. For empty cores, except for the stable compression regime corresponding to sufficiently large values of t/L , the specific strength

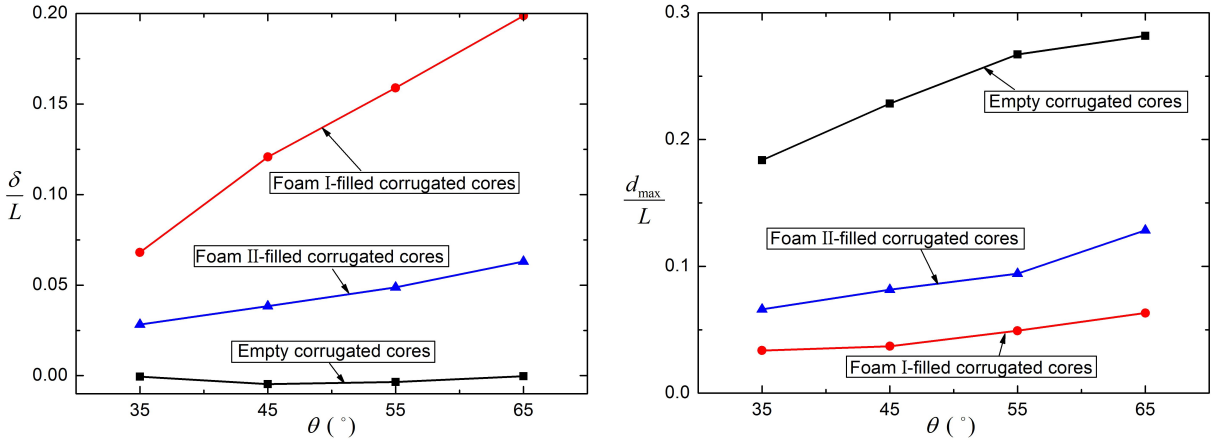


Figure 10. Normalized length reduction (left) and normalized maximum lateral deflection (right) of core web (up to nominal compressive strain of 0.30) plotted as functions of inclination angle for both foam-filled and empty corrugated cores. Core web slenderness ratio fixed at $t/L = 0.02$.

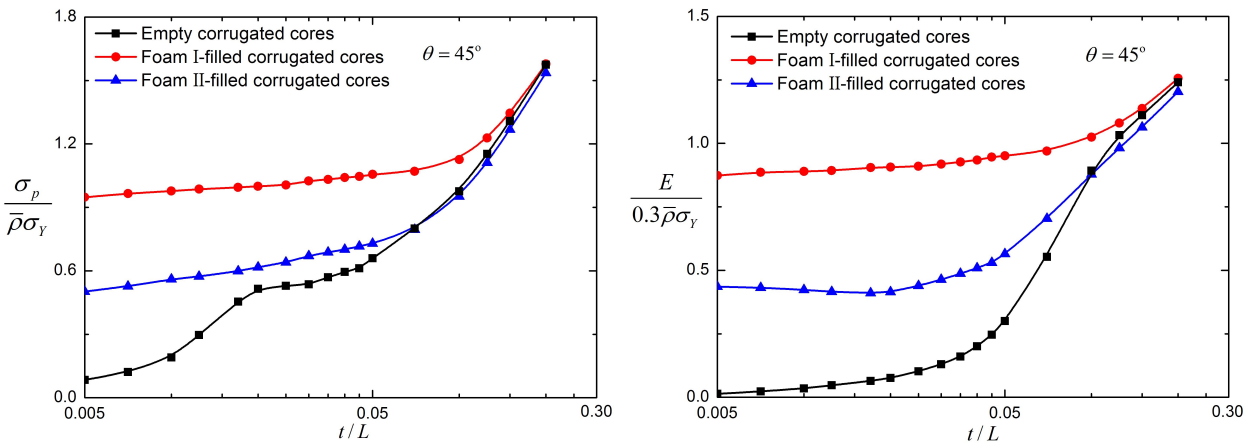


Figure 11. Specific strength (left) and specific energy absorption (right) plotted as functions of core web slenderness ratio t/L for both foam-filled and empty cores, with fixed inclination angle of $\theta = 45^\circ$.

curve may be divided into two distinct regimes corresponding to elastic Euler buckling and plastic buckling of the core web, respectively, the former considerably more steeper than the latter (Figure 11, left). In contrast, with foam filling, the core web collapsed only with plastic buckling, although the types of plastic buckling may be different (see the next section) and hence the specific strength curve was much smoother than that of the empty core.

In terms of compressive strength and energy absorption, the superiority of foam-filled cores over empty ones was the greatest when the core web slenderness ratio was relatively small ($t/L \leq 0.02$). As previously mentioned, within this regime, the collapse mode of the empty core was dominantly elastic

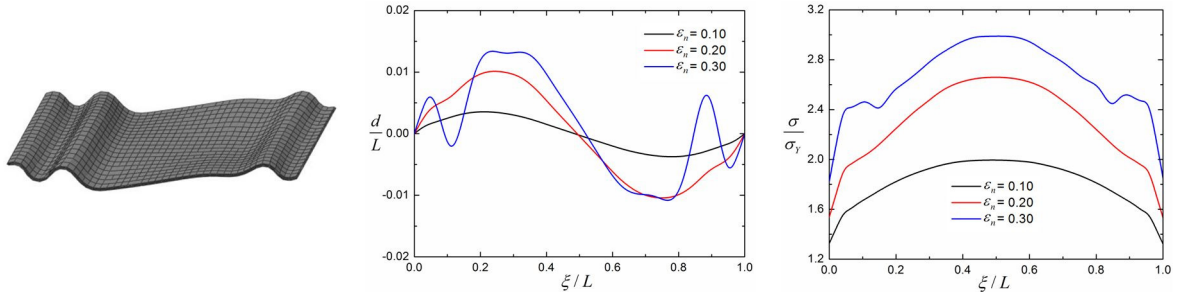


Figure 12. Sides local-buckling: $t/L = 0.007$, $\theta = 45^\circ$, foam I-filled corrugated core.

Euler buckling. In sharp contrast, at large values of $t/L (> 0.1)$, stable compression with plastic hardening occurred in both empty and foam-filled cores, and the strengthening effect of foam filling gradually vanished (Figure 11).

The results of Figure 11 revealed that the beneficial effect of foam filling on specific energy absorption was more obvious than that on specific strength. The foam fillers not only greatly delayed core web buckling and elevated the compressive strength, but also improved significantly the flow stress of post-buckling [Ostos et al. 2012].

4.2. Collapse modes and collapse mechanism maps. Under quasistatic out-of-plane compression, extensive FE simulations were carried out to explore how the collapse mode of an empty corrugated core would vary when its interstices were filled with aluminum foams. For a given core type (filled or unfilled), the dependence of its collapse mode on inclination angle θ and core web slenderness ratio t/L was also determined. As the deformation state at peak load was not obvious especially for foam I-filled cores, the selected collapse modes presented in Figures 12–16 all corresponded to $\epsilon_n = 0.30$ in the post-buckling regime. For comparison, the two typical collapse modes shown in Figures 17–18 for the empty core were also calculated at $\epsilon_n = 0.30$.

For simplicity, the middle axial line of the core web located at the central cross section of the RVE was selected as the analysis object. In Figures 12–18, together with the collapse modes given in the left-most parts, the evolution of deformation and von Mises stress along such middle line for each mode were separately plotted in the middle and right-most parts for selected nominal strain levels. In these figures, ξ/L denoted the relative location of an arbitrary point along the middle line of the core web, whilst d/L and σ/σ_Y represented the normalized lateral deflection and normalized equivalent stress of the corresponding point, respectively.

It should be pointed out that the present study did not cover thin-walled ($t/L < 0.005$) and thick-walled ($t/L > 0.3$) corrugated plates, as the buckling of thin plates was highly imperfection sensitive whilst the use of thick plates was limited for weight-sensitive applications. Further, within the regime of $t/L < 0.005$, the collapse was governed by plasticity-moderated elastic buckling and it was problematic to obtain accurate FE results, analogous to thin-walled tubes [Pingle et al. 2011].

4.2.1. Collapse modes of foam-filled corrugated core. Under quasistatic out-of-plane compression, as the values of t/L and θ were systematically varied, a total of five distinct collapse modes, denoted separately as A, B, C, D and E, were identified for the foam-filled corrugated cores, as shown in Figures 12–16.

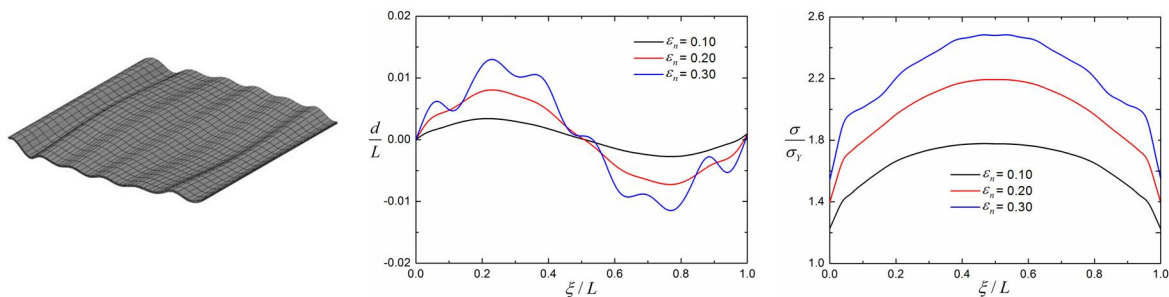


Figure 13. Plastic wrinkling: $t/L = 0.006$, $\theta = 35^\circ$, foam I-filled corrugated core.

For each collapse mode, its regime of dominance was marked on the collapse mechanism map, which was plotted in Figure 19 on a chart of t/L and θ . The characteristics of each mode were discussed below.

Mode A: sides local-buckling. Such buckling mode may occur only in foam I-filled corrugated cores having small values of t/L and inclination angle larger than 35° (Figure 19, top left). As shown in Figure 12, localized plastic hinges emerged only near the ends of the corrugated plate and did not expand to the middle region. Since t/L was small, the lateral support provided by the relatively dense foam I (versus foam II) to the corrugated plate was large, preventing its bending deformation in the middle region. In contrast, towards the ends of the plate, the constraint was not strong enough, causing localized buckling as well as fluctuation of the von Mises equivalent stress in this region (Figure 12, right). This particular buckling mode may be attributed to the heterogeneous distribution of foam constraints on the deformation (deflection) and buckling of the corrugated plate.

Mode B: plastic wrinkling. The mode of “plastic wrinkling” could occur in corrugated plates having small values of t/L (less than 0.015) and filled with either foam I with small inclination angles (less than 45° ; see Figure 19, top left) or foam II (Figure 19, top right). This collapse mode appeared with small buckle waves along with global odd-symmetrical bending, similar to a dual-frequency buckling mode, as illustrated in Figure 13 (left). Interestingly, due to the early formation of global bending, wrinkling with small buckle wave length appeared along with one complete sine-wave shape at large strain (Figure 13, middle), which was quite different from the traditional wrinkling [Hadi 2001]. The equivalent stress exhibited only slight fluctuations (Figure 13, right) due to the relatively small lateral deflections (Figure 13, middle) of the corrugated plate associated with wrinkling.

Mode C: middle local-buckling. As shown in Figure 19 (top: left and right), at intermediate values of t/L the corrugated plates in a foam-filled core may collapse with the mode of “middle local-buckling”. Different from “sides local-buckling”, a pair of localized plastic hinges formed only in the middle portion of the plate (Figure 14, left). Before the collapse occurred, the corrugated plate (its middle region in particular) behaved approximately as a straight line, with nearly identical equivalent stress in this region. As the strain was increased, a couple of localized plastic hinges were developed close to the middle region where much bending occurred while the remaining parts of the plate rotated around these hinges as rigid rods (Figure 14, middle). Simultaneously, such local-buckling induced abrupt fluctuation of the equivalent stress in the middle region (Figure 14, right). During post-buckling, the equivalent stress in the

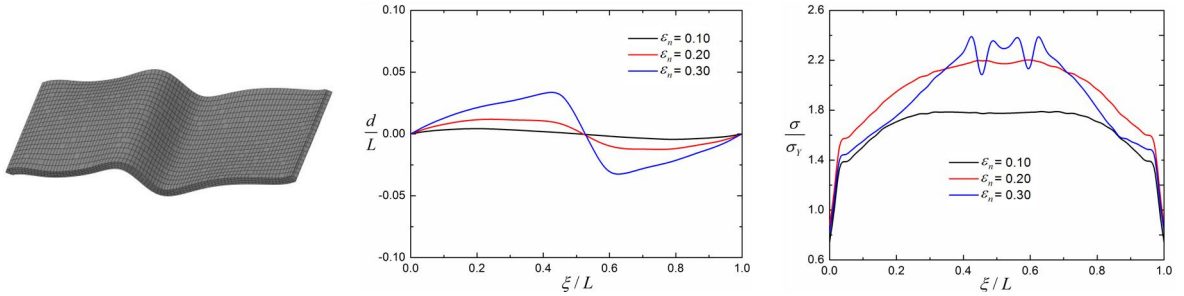


Figure 14. Middle local-buckling: $t/L = 0.02$, $\theta = 65^\circ$, foam I-filled corrugated core.

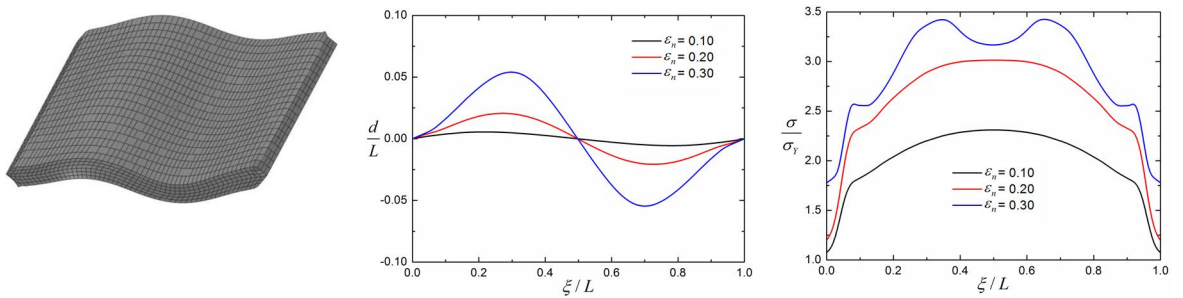


Figure 15. Plastic odd-buckling: $t/L = 0.06$, $\theta = 55^\circ$, foam I-filled corrugated core.

parts of the corrugated plate without plastic hinges even decreased due to relaxation of the compressive stresses (Figure 14, right).

Mode D: plastic odd-buckling. As the values of t/L became larger than those corresponding to mode C (Figure 19, top: left and right), different from the collapse mode of “plastic wrinkling”, a kind of global plastic buckling mode appeared as a single-frequency wave in an odd-symmetrical way; see Figure 15 (left). Whilst the corrugated plate only exhibited a slight bending trend before the collapse, its lateral deflection increased rapidly once buckling occurred; see Figure 15 (middle). Correspondingly, during post-buckling, the fluctuation of the equivalent stress occupied the main region of the plate; see Figure 15 (right). To avoid confusion with the plastic buckling of empty corrugated plates (see immediately below), the plastic buckling mode as characterized above was defined here as *plastic odd-buckling*.

Note that the above four types of collapse mode for foam-filled corrugated plates all occurred at compressive strains significantly larger than those associated with empty ones, consistent with the results presented in the previous section.

Mode E: stable compression. As the value of t/L became sufficiently large, the stubby thick-walled corrugated plates in a foam-filled core did not collapse but rather deform in “stable compression” with continuously plastic hardening (Figure 16, left). Despite of the slight bending due to the strong constraint of the clamped ends, the equivalent stress in the main middle region of the corrugated plate was almost identical throughout the compression process (Figure 16, right). This collapse mode also occurred in the empty cores, as shown in Figure 19 (bottom).

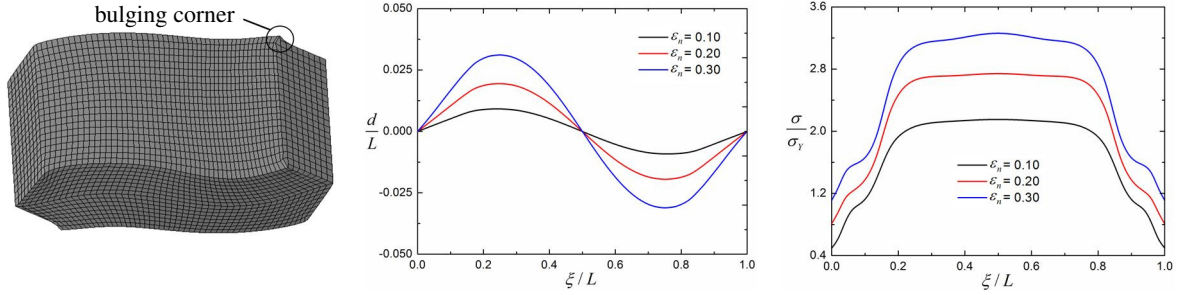


Figure 16. Stable compression: $t/L = 0.20$, $\theta = 45^\circ$, foam I-filled corrugated core.

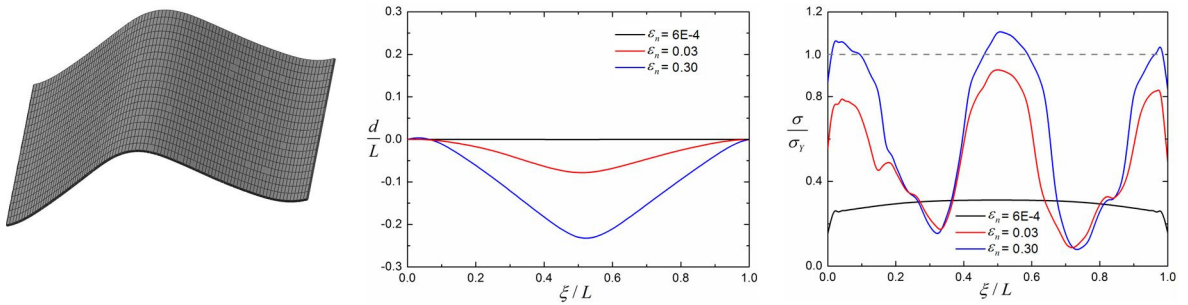


Figure 17. Euler buckling: $t/L = 0.01$, $\theta = 45^\circ$, empty corrugated core.

For the foam-filled cores, four different types of buckling mode had now been identified, including three localized buckling (sides local-buckling, plastic wrinkling and middle local-buckling) and one global buckling (plastic odd-buckling). These collapse modes as illustrated in the left-most parts of Figures 12–15 represented the typical examples marked in Figure 19 where the dominance regime of another collapse mode, stable compression (Figure 16), was also given. Interestingly, the results of Figures 12–16 suggested that the collapse modes of foam-filled cores all exhibited an *odd-symmetry* feature. In contrast, the empty cores collapsed in either elastic or plastic buckling had the common feature of global *even symmetry*, as discussed below.

4.2.2. Collapse modes of empty corrugated core. In addition to stable compression, the present FE simulations revealed that an empty corrugated core could also collapse in two other modes (F and G), defined here as *Euler buckling* and *plastic even buckling*.

Mode F: Euler buckling. For empty cores with small values of t/L (less than 0.018), elastic Euler buckling occurred at small strain levels. As shown in Figure 17, the corrugated plate collapsed with three elastic hinges: one in the middle and the other two near the ends caused by the rotating of the plate. This collapse mode was quite different from that of foam-filled cores, as the constraint provided by filling foam against plate rotation was absent. Moreover, during post-buckling, the elastic hinges became gradually plastic as the strain was increased (Figure 17, right).

Mode G: plastic even-buckling. Different from the mode of plastic odd-buckling in foam-filled cores, an empty core with sufficiently large values of t/L (larger than 0.018) collapsed with plastic buckling in an “even-symmetry” way; see Figure 18 (left). Similar to Euler buckling, three hinges emerged, all

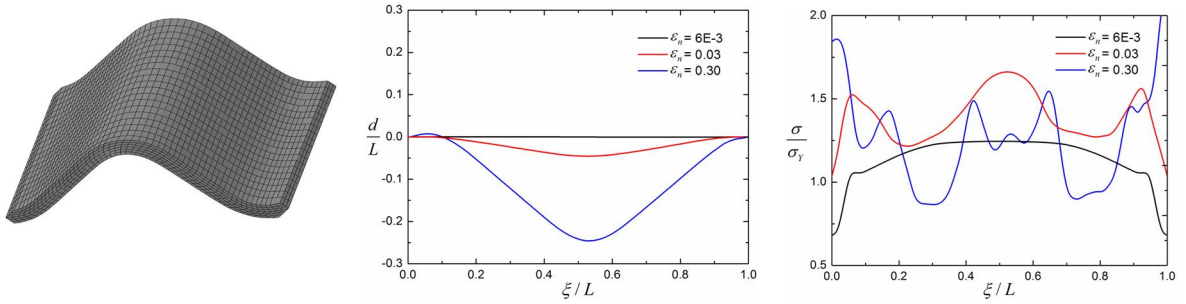


Figure 18. Plastic even-buckling: $t/L = 0.05$, $\theta = 55^\circ$, empty corrugated core.

associated with the equivalent stress exceeding the yield level (Figure 18, right). Unlike the foam-filled cores, within the stage of post-buckling at large compressive strains, the equivalent stress near the two ends of the corrugated plate was larger than that in the center, whether the empty core collapsed with elastic buckling or plastic even-buckling.

It was of interest to notice that, for a thick-walled corrugated plate under large compressive strain, small yet visible corner bulging occurred, as illustrated in Figure 16 (left). The bulging was caused by the material located inside the core (along direction-1) being squeezed out, analogous to the case of a thick-walled short tube under internal or external pressure [Zhu et al. 2013]. Whilst the bulging corner occurred in either foam-filled or empty corrugated cores, the extent of bulging was more serious for the former due to the additional squeezing of the filling foam.

It was seen from Figure 19 (top: left and right) that whilst the collapse modes of corrugated plates filled with either foam I or foam II were more or less similar (yet totally different from the traditional Euler buckling and plastic buckling of empty plates), the regime of dominance of each mode (apart from stable compression) varied considerably as foam I was replaced by foam II. In particular, with foam II insertions, the mode of “sides local-buckling” was absent; see Figure 19 (top right). Further, the regimes of collapse modes for empty cores were nearly independent of the inclination angle θ whereas those of the foam-filled cores were quite sensitive to θ .

4.2.3. Collapse mechanisms. The deformation and collapse of a foam-filled corrugated core may be attributed to the synergetic effects of several factors, including: constraints of foam insertions; nonuniformity of foam constraints; influence of core web slenderness ratio t/L and inclination angle θ . Although different collapse modes were identified for foam-filled cores, the global tendency of the deformation was similar, all exhibiting an odd-symmetry feature. Qualitatively, this may be interpreted as follows. Analogous to the analysis of Yoo et al. [2010] for foam-filled egg-boxes, the difference in densification strain on the two sides of the corrugated plate led to unbalanced forces on either side of the plate, as illustrated in Figure 20 (top left). Only near the center of the plate were the stresses from the foam on either side of the plate expected to be equal. Hence, in contrast to the even-symmetrical bending of empty corrugated plates, there was tendency for the foam insertions to generate a rotational moment, inducing odd-symmetrical (or antisymmetrical) buckling of the plate as shown in Figure 20 (right).

4.3. Strength maps. For both empty and foam-filled corrugated cores, contours of their relative strength σ_p/σ_Y as well as relative density $\bar{\rho}$ were plotted in Figure 21 on a chart with axes of t/L and θ . The

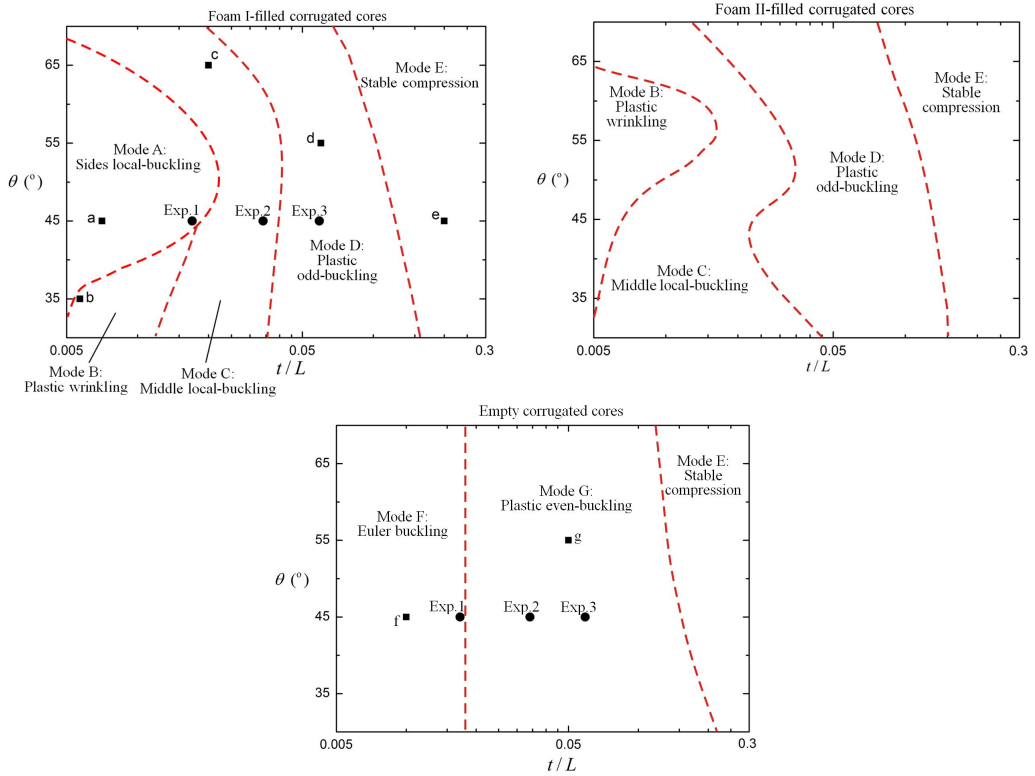


Figure 19. Collapse mechanism map for corrugated plates filled with: foam I (top left); foam II (top right); no foam (bottom). Red dashed lines separated neighboring deformation modes. Experimental data were marked as solid circles at top left and bottom, whilst typical geometries for different deformation modes were marked as solid squares. Boundary between elastic and plastic buckling for empty corrugated plates was constructed using (A.4).

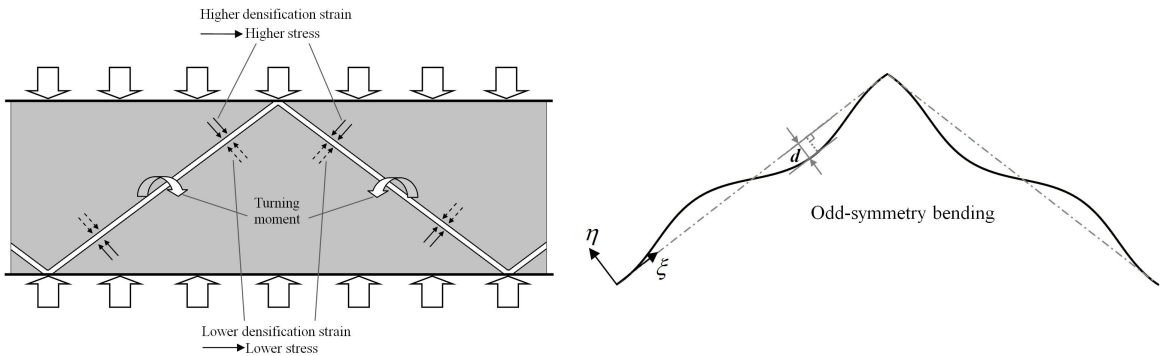


Figure 20. Schematic of global bending deformation of foam-filled corrugated plates under out-of-plane compression. Left: emergence of turning (bending) moment on corrugated plate; right: corresponding global bending deformation of corrugated plate (middle line).

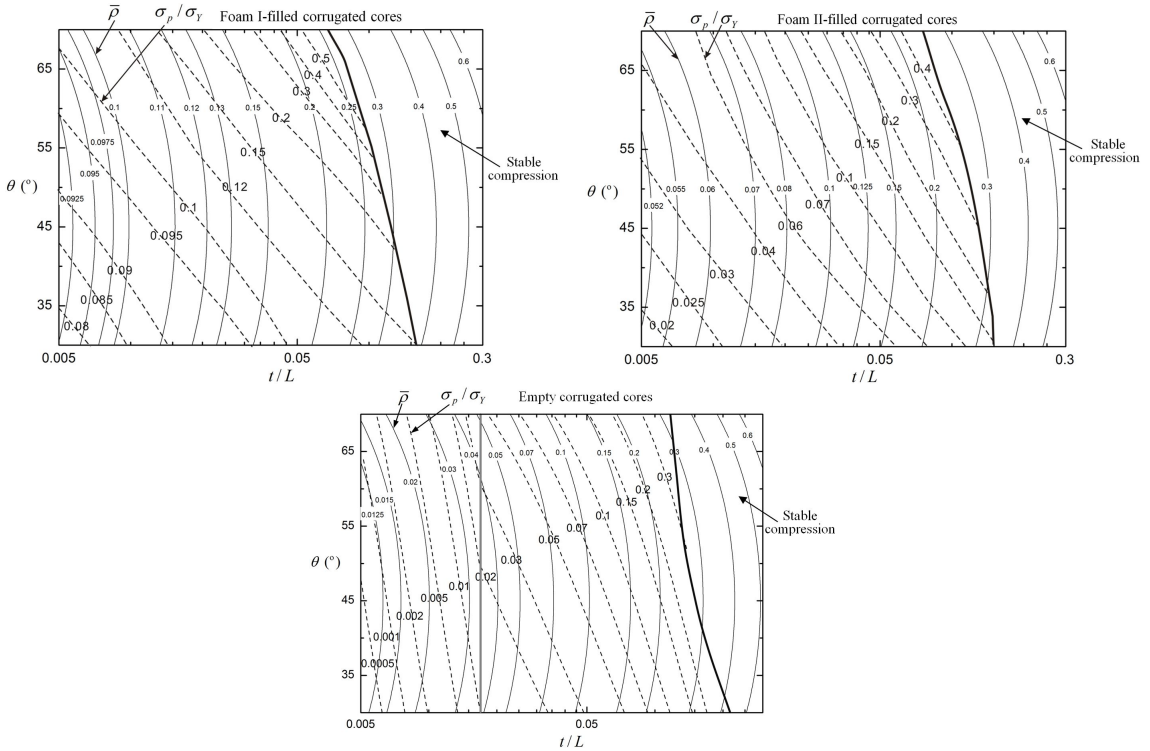


Figure 21. Normalized peak stress (σ_p/σ_Y) and relative density ($\bar{\rho}$) plotted as functions of core web slenderness ratio (t/L) and inclination angle (θ) for corrugated sandwich plates having: foam I-filled core (top left); foam II-filled core (top right); empty core (bottom). Thick solid lines separated the “stable compression” regime from the plastic buckling modes. Solid contours denoted $\bar{\rho}$ and dashed lines denoted σ_p/σ_Y .

thick inclined line on the chart separated the “stable compression” regime which exhibited no peak stress from the buckling regime where the peak stress was clearly defined.

Consider a trajectory of fixed $\bar{\rho}$ for the foam-filled cores. The relative strength σ_p/σ_Y increased monotonously with increasing θ , rather than increasing t/L . Consequently, there existed no clear optimal path of core geometry that gave rise to the peak stress for any given value of $\bar{\rho}$ that maximized the peak stress. This indicated that θ played a more important role than t/L in the compressive response of foam-filled cores. It followed that, for out-of-plane compression, it would be better to design a foam-filled corrugated core with large inclination angle, with θ close to 90 degree being the best choice. In reality, however, it was difficult to fabricate corrugated cores without using platforms when θ was larger than say 70 degree. Further, in addition to out-of-plane compression, the performance of foam-filled cores having large inclination angles subjected to other loading types such as three-point bending and shear needs to be considered.

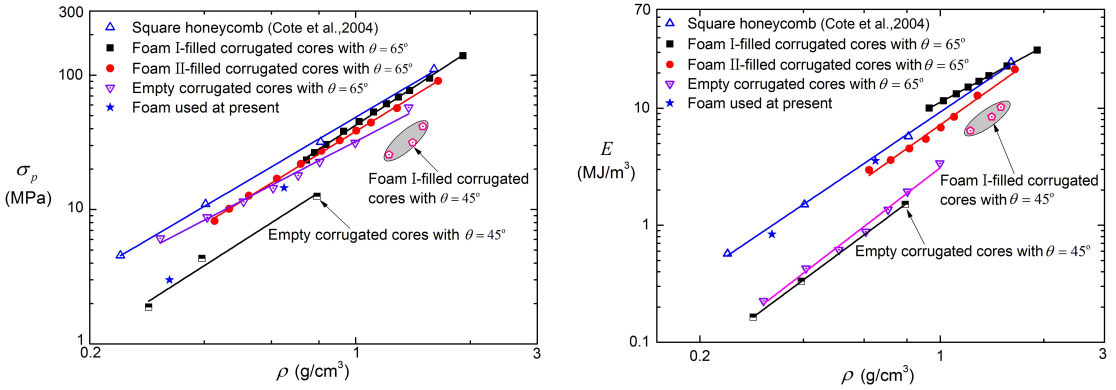


Figure 22. Left: Performance of competing sandwich core topologies under quasistatic compression: peak stress (compressive strength) versus core density; right: energy absorption per unit volume (up to $\epsilon_n = 0.30$) versus core density. Except for the results of square honeycombs from [Côté et al. 2004], all the other data was from the present study.

5. Comparison with competing core topologies

Under out-of-plane compression, the energy absorption capacity of a sandwich core was traditionally defined as the integration of stress with respect to strain from 0 up to 0.50. However, as the present study of different sandwich cores was limited to the nominal compressive strain of $\epsilon_n = 0.30$, for consistency the energy absorption per unit volume was defined as

$$E = \int_0^{0.30} \sigma_n d\epsilon_n. \quad (10)$$

Figure 22 compared separately the compressive strength (peak stress) and energy absorption of foam-filled corrugated cores with several competing core topologies for lightweight sandwich constructions, including close-celled metallic foams, square honeycombs and empty corrugated cores. Both experimental data and FE simulation results were used for the comparison. For foam-filled cores, data for both foam I and foam II insertions were presented. Further, for both empty and foam-filled cores, results for $\theta = 45^\circ$ as well as $\theta = 65^\circ$ were included.

It was seen from Figure 22 (left) that the compressive strength of foam I-filled core with $\theta = 65^\circ$ was almost comparable with that of square honeycombs [Côté et al. 2004], and considerably superior to either metal foams (used in the present study) or empty corrugated cores. Further, for a fixed core density, foam I-filled core with $\theta = 65^\circ$ performed much better than that with $\theta = 45^\circ$, consistent with previous results concerning the effect of inclination angle.

In addition to compressive strength, the energy absorption of foam I-filled sandwich core with $\theta = 65^\circ$ also exceeded that of square honeycombs; see Figure 22 (right). Square honeycombs rapidly softened due to buckling once the peak stress was reached, whilst the softening of foam-filled corrugated cores ($\theta = 65^\circ$) after the peak was less pronounced. In addition, the post-buckling performance was also considerably strengthened by the filling foam relative to the unfilled cores.

6. Conclusions

Detailed physical mechanisms underlying the significant beneficial effects of filling aluminum foams into the interstices of corrugated plates made of 304 stainless steel were exploited by using the finite element method. With the focus placed upon quasistatic out-of-plane compression, the beneficial effects were assessed on the basis of elevated peak stress and energy absorption relative to unfilled corrugated plates of equal mass. The main findings were summarized as follows:

- (1) Good agreement between FE simulated and experimentally measured stress versus strain curves was achieved. The deformation and collapse modes of both the empty and foam-filled corrugated plates were also accurately captured by the FE simulations.
- (2) The post-yielding strength and energy absorption of foam-filled corrugated plates were significantly enhanced relative to empty ones, both exceeding the combined contributions from the corrugated plates and the foam alone, and the advantages increased as the foam became denser.
- (3) The coupling effects of a corrugated plate and the surrounding foam resulted in much delayed and stabilized buckling of the former. With foam support, the corrugated plate experienced noticeable length reduction as axial compression was dominant before the plate collapsed. As the plate began to bend, the foam insertions were strengthened, changing the initial state of uniaxial compressive stressing to the state of complex stressing involving compression, tension and shear. In comparison, in the absence of foam filling, the corrugated plate was dominated by bending deformation (with little length change) and easily collapsed, with a tiny critical strain ranging from 0.002 to 0.004.
- (4) The beneficial effects of foam filling to both the strength and energy absorption was the greatest if the slenderness ratio $t/L \leq 0.02$, when the empty corrugated plates collapsed by elastic Euler buckling. For sufficiently large values of t/L , stable compression with plastic hardening of both the empty and foam-filled corrugated plates occurred so that the strengthening effect of foam filling was gradually lost.
- (5) The inclination angle θ also played an important role in dictating the compressive response of both the empty and foam-filled corrugated plates. For the foam-filled corrugated plates, the specific strength and energy absorption depended primarily upon the inclination angle, with a weak dependence upon the core web slenderness.
- (6) Different from the traditional buckling modes of unfilled plates, a variety of different collapse modes were identified for foam-filled plates, including sides local-buckling, plastic wrinkling, middle local-buckling and plastic odd-buckling. Correspondingly, collapse mechanism maps were constructed.

Besides the out-of-plane compressive response, similar beneficial effects had been established when the foam-filled sandwich plates were subjected to three-point bending and simple shear. The varying role of foam insertion with increasing compression velocity had also been explored. These experimental and theoretical results will be reported in separate studies. In summary, the foam-filled corrugated topology is attractive from the perspectives of strength and energy absorption, holding great potential for heavy-duty structural applications.

Appendix: Analytical formulae for buckling of empty corrugated panels

For empty corrugated panels subjected to uniform out-of-plane compression, plane strain assumption was appropriate. Therefore, $(1 - \nu^2)$ was introduced to the Young's modulus E_s of the core web material whilst its yielding stress became $2\sigma_Y/\sqrt{3}$. For core webs having small slenderness ratios, an equilibrium analysis indicated the out-of-plane compressive strength may be expressed as

$$\sigma_{p\text{-empty}} = \sigma_c \tan \theta(t/L) \quad (\text{A.1})$$

where σ_c was the maximum axial compressive stress of the core web. For elasto-plastic hardening materials (i.e., stainless steel as considered in the present study), according to the Euler buckling and Shanley plastic bifurcation stresses [Shanley 1947; Côté et al. 2006], σ_c may be obtained as

$$\sigma_c = \begin{cases} \frac{\pi^2 E_s}{12(1-\nu^2)} \left(\frac{t}{\mu L}\right)^2 & \text{if } \frac{t}{L} < \mu \sqrt{\frac{8\sqrt{3}(1-\nu^2)\sigma_Y}{\pi^2 E_s}}, \\ \frac{\pi^2 E_t}{12} \left(\frac{t}{\mu L}\right)^2 & \text{otherwise,} \end{cases} \quad (\text{A.2})$$

where the coefficient μ was introduced to correct the effective length of the core web under different end constraints. For the core webs considered here, it was reasonable to take the ends of the core web as built-in constrained, giving $\mu = 0.5$. For elastic perfectly plastic materials, the Equation (A.2) may be simplified to

$$\sigma_c = \begin{cases} \frac{\pi^2 E_s}{12(1-\nu^2)} \left(\frac{t}{\mu L}\right)^2 & \text{if } \frac{t}{L} < \mu \sqrt{\frac{8\sqrt{3}(1-\nu^2)\sigma_Y}{\pi^2 E_s}}, \\ \frac{2\sigma_Y}{\sqrt{3}} & \text{otherwise.} \end{cases} \quad (\text{A.3})$$

It followed from Equation (A.2) or (A.3) that the critical slenderness ratio corresponding to the transition from elastic buckling to plastic buckling (or yielding) was

$$\left.\frac{t}{L}\right|_{\text{critical}} = \mu \sqrt{\frac{8\sqrt{3}\sigma_Y(1-\nu^2)}{\pi^2 E_s}}. \quad (\text{A.4})$$

Acknowledgment

This work was supported by the National Basic Research Program of China (2011CB610305), the National Natural Science Foundation of China (11021202, 11072188 and 11102152), and the National 111 Project of China (B06024).

References

- [Burlayenko and Sadowski 2010] V. N. Burlayenko and T. Sadowski, "Effective elastic properties of foam-filled honeycomb cores of sandwich panels", *Compos. Struct.* **92**:12 (2010), 2890–2900.
- [Calladine and English 1984] C. R. Calladine and R. W. English, "Strain-rate and inertia effects in the collapse of two types of energy-absorbing structure", *Int. J. Mech. Sci.* **26**:11–12 (1984), 689–701.

- [Cartié and Fleck 2003] D. D. Cartié and N. A. Fleck, “The effect of pin reinforcement upon the through-thickness compressive strength of foam-cored sandwich panels: porous materials”, *Compos. Sci. Technol.* **63**:16 (2003), 2401–2409.
- [Côté et al. 2004] F. Côté, V. S. Deshpande, N. A. Fleck, and A. G. Evans, “The out-of-plane compressive behavior of metallic honeycombs”, *Mater. Sci. Eng. A* **380**:1–2 (2004), 272–280.
- [Côté et al. 2006] F. Côté, V. S. Deshpande, N. A. Fleck, and A. G. Evans, “The compressive and shear responses of corrugated and diamond lattice materials”, *Int. J. Solids Struct.* **43**:20 (2006), 6220–6242.
- [Deshpande and Fleck 2000] V. S. Deshpande and N. A. Fleck, “Isotropic constitutive models for metallic foams”, *J. Mech. Phys. Solids* **48**:6–7 (2000), 1253–1283.
- [DSSC 2007] DSSC, *ABAQUS/explicit user’s manual version 6.7*, Providence, Rhode Island, USA, 2007.
- [Hadi 2001] B. K. Hadi, “Wrinkling of sandwich column: comparison between finite element analysis and analytical solutions”, *Compos. Struct.* **53**:4 (2001), 477–482.
- [Kazemahvazi and Zenkert 2009] S. Kazemahvazi and D. Zenkert, “Corrugated all-composite sandwich structures, 1: Modeling”, *Compos. Sci. Technol.* **69**:7–8 (2009), 913–919.
- [Kazemahvazi et al. 2009] S. Kazemahvazi, D. Tanner, and D. Zenkert, “Corrugated all-composite sandwich structures. Part 2: Failure mechanisms and experimental programme”, *Compos. Sci. Technol.* **69**:7–8 (2009), 920–925.
- [Li and Muthyala 2008] G. Li and V. D. Muthyala, “Impact characterization of sandwich structures with an integrated orthogrid stiffened syntactic foam core”, *Compos. Sci. Technol.* **68**:9 (2008), 2078–2084.
- [Liu et al. 2008] T. Liu, Z. C. Deng, and T. J. Lu, “Analytical modeling and finite element simulation of the plastic collapse of sandwich beams with pin-reinforced foam cores”, *Int. J. Solids Struct.* **45**:18–19 (2008), 5127–5151.
- [Mahmoudabadi and Sadighi 2011] M. Z. Mahmoudabadi and M. Sadighi, “A study on the static and dynamic loading of the foam filled metal hexagonal honeycomb — theoretical and experimental”, *Mater. Sci. Eng. A* **530**:0 (2011), 333–343.
- [Mamalis et al. 2008] A. G. Mamalis, D. E. Manolacos, M. B. Ioannidis, K. N. Spentzas, and S. Koutroubakis, “Static axial collapse of foam-filled steel thin-walled rectangular tubes: experimental and numerical simulation”, *Int. J. Crashworthiness* **13**:2 (2008), 117–126.
- [Marasco et al. 2006] A. I. Marasco, D. D. R. Cartié, I. K. Partridge, and A. Rezai, “Mechanical properties balance in novel Z-pinned sandwich panels: out-of-plane properties”, *Compos. A Appl. Sci. Manuf.* **37**:2 (2006), 295–302. CompTest 2004.
- [Nanayakkara et al. 2011] A. Nanayakkara, S. Feih, and A. P. Mouritz, “Experimental analysis of the through-thickness compression properties of z-pinned sandwich composites”, *Compos. A Appl. Sci. Manuf.* **42**:11 (2011), 1673–1680.
- [Nia and Sadeghi 2010] A. A. Nia and M. Z. Sadeghi, “The effects of foam filling on compressive response of hexagonal cell aluminum honeycombs under axial loading—experimental study”, *Mater. Design* **31**:3 (2010), 1216–1230.
- [Ostos et al. 2012] J. B. Ostos, R. G. Rinaldi, C. I. Hammetter, G. D. Stucky, F. W. Zok, and A. J. Jacobsen, “Deformation stabilization of lattice structures via foam addition”, *Acta Mater.* **60**:19 (2012), 6476–6485.
- [Pingle et al. 2011] S. M. Pingle, N. A. Fleck, V. S. Deshpande, and H. N. G. Wadley, “Collapse mechanism maps for a hollow pyramidal lattice”, *Proc. R. Soc. Lond. A* **467**:2128 (2011), 985–1011.
- [Rice et al. 2006] M. C. Rice, C. A. Fleischer, and M. Zupan, “Study on the collapse of pin-reinforced foam sandwich panel cores”, *Exp. Mech.* **46**:2 (2006), 197–204.
- [Shanley 1947] F. R. Shanley, “Inelastic column theory”, *J. Aeronaut. Sci.* **14**:5 (1947), 261–268.
- [Tam and Calladine 1991] L. L. Tam and C. R. Calladine, “Inertia and strain-rate effects in a simple plate-structure under impact loading”, *Int. J. Impact Eng.* **11**:3 (1991), 349–377.
- [Vaziri et al. 2006] A. Vaziri, Z. Xue, and J. W. Hutchinson, “Metal sandwich plates with polymer foam-filled cores”, *J. Mech. Mater. Struct.* **1**:1 (2006), 97–127.
- [Wilbert et al. 2011] A. Wilbert, W.-Y. Jang, S. Kyriakides, and J. F. Floccari, “Buckling and progressive crushing of laterally loaded honeycomb”, *Int. J. Solids Struct.* **48**:5 (2011), 803–816.
- [Yan et al. 2013] L. L. Yan, B. Yu, B. Han, C. Q. Chen, Q. C. Zhang, and T. J. Lu, “Compressive strength and energy absorption of sandwich panels with aluminum foam-filled corrugated cores”, *Compos. Sci. Technol.* **86**:0 (2013), 142–148.
- [Yoo et al. 2010] S. H. Yoo, S. H. Chang, and M. P. F. Sutcliffe, “Compressive characteristics of foam-filled composite egg-box sandwich panels as energy absorbing structures”, *Compos. A Appl. Sci. Manuf.* **41**:3 (2010), 427–434.

[Zhang et al. 2013] J. Zhang, P. Supernak, S. Mueller-Alander, and C. H. Wang, “Improving the bending strength and energy absorption of corrugated sandwich composite structure”, *Mater. Design* **52**:0 (2013), 767–773.

[Zhu et al. 2013] Y. Zhu, X. Y. Luo, H. M. Wang, R. W. Ogden, and C. Berry, “Three-dimensional non-linear buckling of thick-walled elastic tubes under pressure”, *Int. J. Non-Linear Mech.* **48**:0 (2013), 1–14.

Received 10 Dec 2013. Revised 28 Mar 2014. Accepted 30 Apr 2014.

BIN HAN: hanbinghost@gmail.com

State Key Laboratory for Strength and Vibration of Mechanical Structures, School of Aerospace, Xi’an Jiaotong University, Xi’an, 710049, China

LEI L. YAN: rayyl@stu.xjtu.edu.cn

State Key Laboratory for Strength and Vibration of Mechanical Structures, School of Aerospace, Xi’an Jiaotong University, Xi’an, 710049, China

BO YU: jo_elnino1987@163.com

State Key Laboratory for Strength and Vibration of Mechanical Structures, School of Aerospace, Xi’an Jiaotong University, Xi’an, 710049, China

QIAN C. ZHANG: zqc111999@mail.xjtu.edu.cn

State Key Laboratory for Strength and Vibration of Mechanical Structures, School of Aerospace, Xi’an Jiaotong University, Xi’an, 710049, China

CHANG Q. CHEN: chencq@tsinghua.edu.cn

Department of Engineering Mechanics, CNMM & AML, Tsinghua University, Beijing, 100084, China

TIAN J. LU: tjlu@mail.xjtu.edu.cn

State Key Laboratory for Strength and Vibration of Mechanical Structures, School of Aerospace, Xi’an Jiaotong University, Xi’an, 710049, China

JOURNAL OF MECHANICS OF MATERIALS AND STRUCTURES

msp.org/jomms

Founded by Charles R. Steele and Marie-Louise Steele

EDITORIAL BOARD

ADAIR R. AGUIAR	University of São Paulo at São Carlos, Brazil
KATIA BERTOLDI	Harvard University, USA
DAVIDE BIGONI	University of Trento, Italy
IWONA JASIUK	University of Illinois at Urbana-Champaign, USA
THOMAS J. PENCE	Michigan State University, USA
YASUhide SHINDO	Tohoku University, Japan
DAVID STEIGMANN	University of California at Berkeley

ADVISORY BOARD

J. P. CARTER	University of Sydney, Australia
D. H. HODGES	Georgia Institute of Technology, USA
J. HUTCHINSON	Harvard University, USA
D. PAMPLONA	Universidade Católica do Rio de Janeiro, Brazil
M. B. RUBIN	Technion, Haifa, Israel

PRODUCTION production@msp.org

SILVIO LEVY Scientific Editor

Cover photo: Mando Gomez, www.mandolux.com

See msp.org/jomms for submission guidelines.

JoMMS (ISSN 1559-3959) at Mathematical Sciences Publishers, 798 Evans Hall #6840, c/o University of California, Berkeley, CA 94720-3840, is published in 10 issues a year. The subscription price for 2014 is US \$555/year for the electronic version, and \$710/year (+\$60, if shipping outside the US) for print and electronic. Subscriptions, requests for back issues, and changes of address should be sent to MSP.

JoMMS peer-review and production is managed by EditFLOW[®] from Mathematical Sciences Publishers.

PUBLISHED BY

 **mathematical sciences publishers**
nonprofit scientific publishing
<http://msp.org/>

© 2014 Mathematical Sciences Publishers

- Random vibration of shear deformable FGM plates** **VEDAT DOGAN 365**
- Mechanical behavior of brick masonry panels under uniaxial compression**
HACER BILIR ÖZHAN and ISMAIL HAKKI CAGATAY 385
- Collapse mechanisms of metallic sandwich structures with aluminum foam-filled corrugated cores** **BIN HAN, LEI L. YAN, BO YU, QIAN C. ZHANG, CHANG Q. CHEN and TIAN J. LU 397**
- Representative volume element in 2D for disks and in 3D for balls** **NATALIA RYLKO 427**
- Small amplitude elastic buckling of a beam under monotonic axial loading, with frictionless contact against movable rigid surfaces**
FRANCESCO GENNA and GUIDO BREGOLI 441